STING agonists drive recruitment and intrinsic type I interferon responses in monocytic lineage cells for optimal anti-tumor immunity[1]

Authors: Melanie Girard*‡, Tianning Yu*‡, Nathalia V Batista*, Karen K. M. Yeung*, Sara Lamorte†, Wenting Gao*, Miaoxi Liu*2, Tracy L. McGaha*,†, and Tania H. Watts*3

Affiliations:

* Department of Immunology, University of Toronto, Toronto, Canada.

†Tumor Immunotherapy Program, Princess Margaret Cancer Centre, University Health Network, Toronto, Canada.

‡Co-first authors.

Corresponding author: Dr. Tania H. Watts, Department of Immunology, University of Toronto, 1 King's College Circle, Toronto, ON M5S 1A8, Canada. E-mail address: tania.watts@utoronto.ca

Tel 416-978-4551

Running title: Monocytes lineage cells in STING agonist therapy

Abstract

The cyclic GMP-AMP synthase-stimulator of interferon genes (cGAS-STING) pathway, a sensor of cytosolic DNA, orchestrates the production of pro-inflammatory cytokines, chemokines, and type I interferons (IFN-I), thereby contributing to spontaneous tumor surveillance. Intratumoral delivery of synthetic STING agonists induces IFN-I dependent tumor regression in preclinical cancer models and is being tested clinically. In this study, we investigate the role of monocytic lineage (MCs) cells in response to STING agonist induced IFN-I signaling. We show that CCR2-deficient mice, lacking inflammatory MCs in the periphery, or Lyz2-Cre-IFNAR1$^{fl/fl}$ mice in which IFN-I signaling in monocytes is reduced, exhibit impaired responses to STING agonist therapy of MC38 and/or B16F10 tumors. STING agonist treatment induced CCR5-dependent migration of MCs carrying tumor antigen from the tumor to the lymph nodes. Single-cell RNA sequencing of CD45^{+} cells from lymph nodes and tumors of mice in which half the hematopoietic cells lack the interferon alpha/beta receptor 1 (IFNAR1) revealed that STING agonist therapy induces intrinsic IFNAR1-dependent acquisition of an inflammatory monocytic cell phenotype distinct from inflammatory cDC and a reduction in macrophages with a pro-tumor TGFβ/angiogenesis transcriptome. IL-18 - IL-18R1 interaction was the top predicted interaction between monocytic lineage cells and CD8^{+} T cells or NK cells. Blocking IL-18 reduced IFN-γ production by CD8 T cells in LNs and decreased the therapeutic efficacy of STING agonist treatment in CCR2$^{+/+}$ but not in CCR2$^{-/-}$ mice. These findings support a pivotal role for IL-18 producing inflammatory monocytic lineage cells in CD8 T cell control of melanoma following STING agonist treatment.

47 **Introduction**

48 Monocytic lineage cells (MC), including monocytes, monocyte-derived dendritic cells (DCs) and
49 monocyte-derived macrophages, are highly plastic innate immune cells that adopt distinct
50 functional features depending on the extracellular cues they receive. When MCs enter tumors, they
51 respond to signals from the tumor microenvironment (TME) and differentiate into tumor
52 associated macrophages (TAMs), where they promote tumor progression by suppressing anti-
53 tumor T cell and NK cell responses, and by increasing angiogenesis, tumor cell proliferation and
54 metastasis (1-3). In other contexts, such as during acute viral infections, MCs enter inflamed
55 tissues and respond to proinflammatory cytokines such as type I interferons (IFN-I). These
56 inflammatory monocytic lineage cells (infMCs) help mount effective innate and adaptive immune
57 responses through antigen presentation, co-stimulation, and cytokine production (4-9).

58

59 The cyclic GMP-AMP synthase-stimulator of interferon genes (cGAS-STING) pathway elicits an
60 immune response upon the detection of cytosolic DNA (10-13). Upon binding of double-stranded
61 DNA, cGAS catalyses the formation of 2'3' cyclic GMP-AMP (cGAMP) from cytosolic ATP and
62 GTP molecules (12, 13). cGAMP then binds to the STING adaptor located in the endoplasmic
63 reticulum membrane. This activates NF-κB and IRF3 transcriptional pathways, leading to the
64 production of IFN-Is and other pro-inflammatory cytokines that drive immune responses against
65 viral infection and cancer (10-13).

66

67 Sensing of tumor cell-derived DNA via the cGAS-STING pathway in antigen presenting cells is
68 required for spontaneous priming of anti-tumor $CD8^+$ T cells (14). Moreover, DNA sensing
69 through STING and IFN-I production is required for anti-tumor immune responses induced by

70 radiation therapy and chemotherapy (15). These findings prompted the development of small
71 molecules that could activate the STING-IFN-I pathway for cancer immunotherapy. Activation of
72 STING-IFN-I pathway for cancer immunotherapy has shown promising results in pre-clinical
73 mouse models (16-23). However, to date, clinical trials of STING agonists as monotherapy have
74 shown disappointing results (24), highlighting the need to fully understand the mechanisms of
75 protection in the mouse models to facilitate design of optimized combination therapies. ADU-
76 S100 is a synthetic STING agonist that binds to and activates mouse and human STING and leads
77 to downstream IFN-I production (16, 18). Intra-tumoral administration of ADU-S100 induces
78 tumor regression and systemic protection against tumor re-challenge in mice (16, 18). This effect
79 is mediated through $CD8^+$ T cells and/or NK cells depending on tumor-specific features such as
80 MHC class I expression (16, 21). $BATF3^+$ DCs and IFN-I signaling in cDCs are also required for
81 optimal response to treatment, due to their role in cross-presentation and IL-15 trans-presentation
82 (16, 21). There is a well-established role for IFN-I signaling in the response to STING agonist
83 therapy, as IFNAR1 deficiency or IFN-I neutralization significantly impairs tumor control, $CD8^+$
84 T cell and NK cell responses upon treatment (16, 18, 21).
85
86 Depletion of phagocytic cells using clodronate liposomes can reduce the therapeutic efficacy of
87 STING agonist therapy, suggesting that monocytes and/or macrophages are required for the anti-
88 tumor effects of STING agonists (23, 25, 26). Tumor monocytes accumulating in tumors show
89 transcriptional changes following intra-tumoral STING agonist administration (23, 25, 26).
90 Moreover, monocyte depletion impairs STING-dependent radiation therapy (26). However, to
91 what extent these changes are driven by intrinsic IFN-I signaling and whether IFN-I responses in

92 monocytic lineage cells are required for the therapeutic efficacy of synthetic STING agonists has
93 not been directly tested.
94
95 To address these questions, we investigated the role of intrinsic IFN-I signaling in MCs during
96 intra-tumoral STING agonist therapy of B16F10 tumors using single cell sequencing and
97 multiparameter flow cytometry. We report that intra-tumoral injection of ADU-S100 drives the
98 accumulation of $CD26^{lo}CD11b^{+}Ly6C^{hi}CD64^{+}MAR\text{-}1^{+}$ infMCs in the lymph nodes (LNs) and
99 tumors of mice. CITE-sequencing of LN and tumor cells from IFNAR1 mixed bone marrow
100 chimeric mice shows that infMCs that accumulate following STING agonist administration have
101 a transcriptional program almost entirely dependent on intrinsic IFN-I signaling and characterized
102 by high expression of IL-18 and genes involved in MHC I-restricted presentation. *Ccr2*$^{-/-}$ and
103 *Ifnar1*$^{fl/fl}$ *Lyz2-Cre* mice show impaired response to STING agonist therapy compared to littermate
104 controls, suggesting that MC and MC intrinsic IFN-I responses are required for optimal response
105 to treatment. Mechanistically, we found that neutralization of IL-18 reduced the therapeutic
106 efficacy of STING agonists in *Ccr2*$^{+/+}$ but not *Ccr2*$^{-/-}$ mice and decreased CD8 T cell production
107 of IFN-γ , highlighting the importance of this monocyte-derived pro-inflammatory cytokine during
108 STING agonist therapy of cancer. Taken together, these data suggest that recruitment of MCs and
109 IFN-I-induced IL-18 production by infMCs are pivotal for CD8 T cell control of melanoma
110 following STING agonist therapy.
111
112
113
114

115 **MATERIALS AND METHODS**

116 *Mice.* C57BL/6 and CD45.1 mice were purchased from Charles River Laboratories. *Ifnar1*$^{-/-}$, *Ccr2*$^{-}$
117 $^{/-}$, *Ifnar1*$^{fl/fl}$ and *Lyz2-Cre* mice were purchased from The Jackson Laboratory. *Ccr2*$^{+/-}$ mice were
118 bred to generate *Ccr2*$^{+/+}$ and *Ccr2*$^{-/-}$ littermate controls. *Ifnar1*$^{fl/fl}$ and *Lyz2-Cre* mice were crossed
119 to generate *Ifnar1*$^{fl/fl}$ and *Ifnar1*$^{fl/fl}$ *Lyz2-Cre* littermate controls. Age and sex-matched male and
120 female mice between 6 and 10 weeks of age were enrolled in experiments. Mice were housed
121 under specific pathogen-free conditions. Animal studies were approved by the animal care
122 committee of the University of Toronto in accordance with the Canadian Council on Animal care.
123

124 *Cell culture*. B16F10 cells obtained from the American Type Culture Collection and B16F10.OVA
125 (B16.OVA) was obtained from Dr. Mikael Karlsson, Karolinska Institute. B16.OVA.tomato was
126 generated using the Sleeping Beauty transposon system (Addgene #60513). The MC-38 cell line
127 was obtained from Dr Jean Gariépy at the Sunnybrook Research Institute, Toronto. The cell lines
128 were maintained at 37°C with 5% CO2 in complete Dulbecco's modified Eagle's medium [10%
129 heat-inactivated fetal bovine serum (FBS), streptomycin (100 mg/ml), and penicillin (100 mg/ml);
130 Gibco].
131

132 *In vivo tumor experiments*. Mice were anesthetized with 2-3% isoflurane and 10^6 B16.OVA, $2x10^6$
133 B16.OVA.tomato or 0.5 x 10^6 MC-38 cells were inoculated intradermally or subcutaneously on
134 the right flank in 50 µl D-PBS. Where relevant, mice were randomized into groups with similar
135 average tumor sizes on the day of treatment. When tumors reached an average volume of 100 mm^3,
136 25 µg of ADU-S100 (MedChemExpress) was administered intratumorally in 50 µl D-PBS. An
137 equal volume of DMSO dissolved in D-PBS was used as vehicle control. Tumor volumes were

138 determined with calipers and the formula (length x width^2) x 0.5. Mice were euthanized when
139 tumors reached >1500 mm^3 or were severely ulcerated. For CCR5 blocking experiments,
140 B16.OVA.tomato tumor-bearing C57BL/6 mice were given 10mg/kg maraviroc or PBS treatment
141 4 hours prior to ADU-S100 or vehicle treatment. LNs were collected for flow cytometry on day 1
142 post-treatment.
143
144 *Tissue processing*. Tumors were resected and cut into small pieces and digested in 1 ml HBSS
145 with 825 U/ml collagenase IV (Invitrogen) and 0.1 mg/ml DNAse I for 30 min at 37°C 250 rpm.
146 Tumor cell suspensions were mashed through a 70 µM strainer, washed once in RPMI 10% FBS
147 and resuspended at 100 mg of tumor/ml in D-PBS. Tumor-draining inguinal LNs on the same side
148 as the tumor were mechanically disrupted through a 70 µM strainer to obtain single-cell
149 suspensions.
150
151 *Flow cytometry*. For flow cytometry, 2 x 10^6 cells from the LN or 25 mg of tumor were used per
152 stain. Cells were stained for 15 minutes in eF506 Viability Dye diluted in D-PBS, washed, and
153 treated with Fc-receptor blocking antibodies anti-CD16/CD32 for 10 minutes (Invitrogen). Cells
154 were then stained with cell surface antibodies for 30 minutes, washed and fixed for 10 minutes in
155 Cytofix buffer (BD) at 4°C. For tetramer staining, cells were stained for 30 minutes with H-
156 2K^b/SIINFEKL-APC tetramers at room temperature before carrying out cell surface staining as
157 described above. Anti-CD8a clone KT15 was used when staining with tetramers to prevent non-
158 specific binding of H-2K^b tetramers that can occur with clone 53-6.7. For intracellular staining of
159 nuclear proteins, cells were fixed and permeabilized with Foxp3 transcription factor staining buffer
160 (Invitrogen) for 40 minutes prior to intracellular staining for 30 minutes at 4°C. For intracellular

161 cytokine staining, cells were re-stimulated with 0.1 μM Trp-2 peptide for 6 hours prior to surface
162 staining, then were fixed and permeabilized with Cytofix/Cytoperm buffer (BD) for 20 minutes
163 prior to intracellular cytokine staining for 30 minutes at 4ºC. Data were acquired on a LSR Fortessa
164 X-20 or FACSymphony A3 using FACSDiva software (BD Biosciences) and analyzed with
165 FlowJo (TreeStar). Absolute cell numbers in samples were determined using 123count eBeads
166 (Invitrogen).
167
168 *Ifnar1 mixed bone marrow chimeras.* CD45.1/.2 mice were irradiated with two doses of 550 rad
169 with a 4h rest between doses, and the bone marrow was reconstituted by intravenous injection of
170 a 1:1 mixture of *Ifnar1*$^{+/+}$ CD45.1 and *Ifnar1*$^{-/-}$ CD45.2 bone marrow cells for a total of $5x10^6$
171 cells/mouse. Mice were fed neomycin sulfate water (2 mg/ml) for two weeks following irradiation.
172 Chimerism was assessed in the blood >90 days later, prior to tumor cell inoculation.
173
174 *Sample preparation for CITE-sequencing. Ifnar1* mixed bone marrow chimeras were inoculated
175 with 10^6 B16.OVA cells intradermally and a single dose of ADU-S100 was administered
176 intratumorally on day 12. LNs and tumors were harvested at day 1 and day 2 post-treatment,
177 respectively. LNs were processed as described above. Tumors were digested in HBSS 875 U/ml
178 collagenase IV for 20 min at 37°C 250 rpm, filtered through 70 μM strainers, centrifugated and
179 resuspended at 120 mg/ml in D-PBS. For both the tumor and LN, equal amounts of cell suspension
180 from 3 vehicle or 3 ADU-S100-treated mice were pooled into one vehicle sample and one ADU-
181 S100 sample. Cells were stained with eF506 fixable viability dye in PBS for 10 min on ice, then
182 washed. Fc Receptors were blocked for 10 min before staining with fluor-conjugated antibodies
183 (for FACS) and TotalSeq-A antibodies (Biolegend) in D-PBS 2% FBS for 25 min on ice. Here,

184 vehicle and ADU-S100 treated samples were labeled with distinct hashtag antibodies, while anti-
185 CD45.1 and anti-CD45 barcoded antibodies were used to label *Ifnar1*$^{+/+}$ and *Ifnar1*$^{-/-}$ cells. Cells
186 were washed three times with D-PBS and sorted on a BD FACS Aria IIu (tumor: live CD45^{+} cells;
187 LN: live CD3- CD19- CD11b^{+} and/or MHCII^{+} cells). Vehicle and ADU-S100-treated samples
188 were pooled together at a 1:1 ratio immediately before partitioning on the 10X chromium
189 controller. The Chromium Single Cell 3' Reagent Kits v3.1 were used according to the
190 manufacturer's user guide in conjunction with CITE-seq & Cell Hashing Protocol from the New
191 York Genome Center Technology Innovation Lab. Of note, anti-CD45 clone I3/2.3, anti-CD45
192 clone 30-F11 (in hashtag antibodies), anti-CD45.1 (clone A20) and anti-CD45.2 (clone 104) did
193 not significantly interfere with each other under our experimental conditions.
194
195 *CITE-sequencing analysis.* Sequencing reads from the mRNA library were processed through the
196 Cell Ranger Single Cell Software Suite (10x Genomics) to obtain gene-cell expression matrices.
197 Antibody-derived tags and hashtags were counted using CITE-seq count v1.4.2 and loaded into
198 the Seurat object. RNA, ADT, and HTO expression matrices were imported into RStudio, and
199 downstream analysis was performed using Seurat v3. Cells that expressed fewer than 500 or more
200 than 7000 genes and had a percentage of mitochondrial genes over 10% were filtered out. RNA
201 counts were log-normalized, while antibody-derived counts were normalized using centered log
202 ratio transformation. The 2000 most variable genes were used for dimensionality reduction using
203 principal component analysis. An elbow plot was used to identify the principal components that
204 contribute to most of the variation. For the LN sample, we used the FindNeighbors function using
205 10 dimensions and ran the FindClusters function with a resolution of 0.5. For the tumor sample,
206 we used the FindNeighbors function using 15 dimensions and ran the FindClusters function with

207 a resolution of 0.5. Contaminating T cell, B cell, pDC, NK cell and neutrophil clusters were
208 excluded from the samples and remaining cells were used for analysis. Differential gene
209 expression analysis was performed in Seurat. Genes were considered significantly differentially
210 expressed when they had a $\log_2$ fold-change of > 0.25 and an adjusted p. value < 0.05. To identify
211 enriched gene sets, genes that were differentially expressed across monocyte/macrophage clusters
212 were used as an input for overrepresentation analysis in g: Profiler using Gene Ontology:
213 Biological processes gene sets. The SCENIC workflow was used to predict gene regulatory
214 networks (27). NicheNet was used to predict receptor ligand interactions between cell types (28).
215
216 *In vivo IL-18 blockade.* Mice were administered 200 µg of anti-IL-18 (clone YIGIF74-IG7,
217 BioXCell) or isotype control (clone 2A3, BioXCell) in 100 µl D-PBS intraperitoneally one day
218 before and one day after STING agonist administration.
219
220 *Statistical analysis.* Data were analyzed in GraphPad Prism software (v9.3.1). Student's t-test or
221 one-way ANOVA were used to determine statistical significance as indicated in figure legends.
222 Tumor growth curves were compared using two-way ANOVA with Sidak's multiple comparisons
223 test; the p-value at the last time point is reported. *P < 0.05, **P < 0.01, ***P < 0.001, and ****P
224 < 0.0001 were applied.
225
226 *Data availability statement.* Sequencing data will be made available on gene expression omnibus
227 (GEO). Other data such as flow cytometry FCS files and tumor growth data are available from the
228 authors upon request.
229

230 **Results**

231 *STING agonist treatment induces distinct temporal peaks of MC accumulation in tumors and*
232 *lymph nodes, respectively*

233 Changes in myeloid cell populations in the tumors and tumor-draining LNs of mice were analyzed
234 by flow cytometry following intra-tumoral injection of the STING agonist ADU-S100 into pre-
235 established intradermal B16F10.OVA tumors (**Figure 1A**). One day post-treatment, the number
236 and percentage of migratory cDC1 ($CD26^{+}MHCII^{\mathbf{hi}}CD11c^{+}XCR1^{+}$), migratory cDC2
237 ($CD26^{+}MHCII^{\mathbf{hi}}CD11c^{+}CD172^{+}$) and $Ly6C^{hi}$ MCs ($CD26^{-}CD11b^{+}Ly6G^{-}Ly6C^{hi}$) was
238 significantly increased in the LNs but decreased in the tumors (**Figure 1 B-D, F-G**). However, the
239 number of $Ly6C^{hi}$ MCs in the tumors was restored to initial levels by day 2 post-treatment (**Figure**
240 **1F**). $Ly6C^{hi}$ MCs in the LN and tumor were $CD26^{-}CD88^{+}$ whereas cDCs were $CD26^{hi}CD88^{-}$
241 (**Figure S1A, B**), supporting that these are monocytic lineage cells rather than inflammatory cDCs
242 (29).

243

244 CD64 and MAR-1 staining can be used to identify infMCs in mice, as these antibodies label cells
245 that have responded to inflammatory cytokines and PAMPS (29). While CD64 is an Fc receptor
246 upregulated by monocytes in response to IFN-Is and other pro-inflammatory stimuli, MAR-1 is an
247 antibody clone raised against FcεR1 but that was later found to bind to other Fc receptors including
248 CD64 (29, 30). Here, we used these markers to identify cells that had potentially responded to
249 IFN-Is downstream of intra-tumoral STING agonist administration. We also noted that both the
250 cDC and the $Ly6C^{hi}$ MCs had higher levels of MHC I after ADU-S100 compared to vehicle
251 control, consistent with an IFN-I dependent response (**Figure S1C**). The number and percentage
252 of $Ly6C^{hi}$ MCs positive for CD64 and MAR-1 were significantly increased in the LNs and tumors

253 following STING agonist therapy and peaked at 1- and 2-days post-treatment, respectively (**Figure**
254 **1E, H**). Thus, despite an initial decrease in the number of Ly6C^{hi} MCs in the tumor at day 1 post-
255 treatment, the absolute number of infMCs in tumors was increased by day 2 post-treatment
256 compared to baseline. Taken together, these data show that intra-tumoral administration of ADU-
257 S100 drives the accumulation of CD64^{+} MAR-1^{+} infMCs in the LNs and tumors.
258
259 The ability of Ly6C^{hi} MCs to migrate from tissues to the LN and cross-present antigens during
260 viral infection has been questioned (29, 31). To test if the significantly increased number of Ly6C^{hi}
261 MCs in the LN on day 1 following STING agonist therapy was due to migration from the tumors,
262 wild-type mice were inoculated with B16F10.OVA (B16.OVA) cells that express the red
263 fluorescent protein TdTomato (B16.OVA.tomato) and treated with ADU-S100 or vehicle (**Figure**
264 **1I**). In these mice, intra-tumoral STING agonist injection led to a substantial increase in the
265 number and percentage of tomato^{+} CD26^{-}CD11b^{+}Ly6G-Ly6C^{hi} MCs in the LN (**Figure 1J-K**).
266 We also observed a smaller increase in the number and percentage of tomato^{+} cDC2 (**Figure 1J-**
267 **K**).
268
269 Maraviroc is a CCR5 antagonist that has been shown to block CCR5-dependent monocyte
270 trafficking to the LNs (32). Therefore, to determine if CCR5 plays a role in trafficking of the
271 tomato^{+} CD26^{-}CD11b^{+}Ly6G-Ly6C^{hi} MCs from the tumor to the LN, we treated wild-type mice
272 bearing B16.OVA.tomato tumor with maraviroc or vehicle control, then 4 hours later with ADU-
273 S100 or vehicle and monitored tomato^{+} in the tumor dLN at 24 hours (**Figure 1L**). Consistent with
274 a role for CCR5 in migration of monocytes to LNs, maraviroc treatment substantially reduced
275 accumulation of the tumor antigen bearing monocytes to the dLN (**Figure 1M**). We also noted that

276 LN monocytes from STING agonist treated mice express higher CCR5 than cDC1 and cDC2 at 1
277 day after STING agonist treatment (**Figure 1N**). Taken together, these data suggest that STING
278 agonist treatment induced accumulation of monocytic lineage cells in LN and tumor at different
279 time points, and monocytic lineage cells carry tumor protein to the tumor-draining LN in a CCR5-
280 dependent manner.
281
282 *infMCs are required for optimal tumor control following intra-tumoral STING agonist injection*
283 CCR2 signaling is required for exit of monocytes from the bone marrow (33, 34). To test if CCR2-
284 dependent infMCs play a role in the tumor control induced by STING agonists, we tracked the
285 growth of B16.OVA and MC-38 tumors in *Ccr2*$^{+/+}$ and *Ccr2*$^{-/-}$ littermate mice treated with ADU-
286 S100 or vehicle control. In contrast to *Ccr2*$^{+/+}$ mice, infMCs do not accumulate in the tumors of
287 *Ccr2*$^{-/-}$ mice after STING agonist therapy (**Figure 2A**), whereas tumor accumulation of other
288 immune cell types was unaffected (**Figure S2A, B**). While *Ccr2*$^{+/+}$ and *Ccr2*$^{-/-}$ mice treated with
289 the vehicle control showed no differences in tumor growth, *Ccr2*$^{-/-}$ mice showed impaired tumor
290 control compared to *Ccr2*$^{+/+}$ mice following STING agonist therapy (**Figure 2B, C**).
291
292 STING agonist therapy induces the expansion of tumor specific CD8^{+} T cell and NK cell
293 populations which are measurable as early as 3 days post-treatment (18, 21). To test if monocytes
294 contribute to the proliferation of tumor-specific T cells and NK cells, *Ccr2*$^{+/+}$ and *Ccr2*$^{-/-}$ mice with
295 B16.OVA tumors were sacrificed 3 days post-treatment with STING agonists or vehicle control
296 for flow cytometry analysis. STING agonists significantly increased the proportion of H-2K^{b}
297 SIINFEKL^{+} CD8^{+} T cells and NK cells proliferating in the LN based on Ki-67 staining (**Figure**
298 **2D, E and Figure S2C**). *Ccr2*$^{-/-}$ mice showed reduced Ki67^{+} NK cells (% and mean fluorescence

299 intensity, MFI), but there was no impact on the absolute number of Ki67^{+} NK cells in LN and
300 tumor (**Figure 2E and S2C**). For T cells, although the MFI for Ki67 was decreased in CCR2$^{-/-}$
301 mice, neither the frequency or absolute number of Ki67^{+} cells was significantly impacted by CCR2
302 (**Figure 2D and S2C**). These results may be confounded by the significant apoptosis of
303 lymphocytes in tumors early after ADU-S100 treatment (35). At later time points rapid tumor
304 shrinkage in the *Ccr2*$^{+/+}$ mice precluded accurate T cell measurements. Therefore, to further
305 investigate whether *Ccr2*-deficiency affects early T cell proliferation, we adoptively transferred
306 OT-I T cells into *Ccr2*$^{+/+}$ or *Ccr2*$^{-/-}$ B16.OVA tumor bearing mice 1 day prior to ADU-S100
307 treatment. However, there was no significant impact of *Ccr2* deficiency on LN OT-I T cell
308 proliferation (**Figure S2D**). These data suggest that CCR2-dependent MCs contribute to tumor
309 control but have little or no impact on the initial proliferation of the tumor-specific T cells,
310 suggesting that MCs do not contribute to cross-priming in this model.
311
312 *InfMCs are driven by intrinsic IFN-I signalling during STING agonist therapy*
313 Mice deficient for the interferon alpha/beta receptor 1 (IFNAR1) have sub-optimal responses to
314 STING agonists (16, 18), but whether IFNAR1 signaling within the monocytes promotes anti-
315 tumor immunity in this context is unknown. To address this question, we tracked the growth of
316 B16.OVA tumors in *Ifnar1*$^{fl/fl}$ *Lyz2-Cre* mice, which have lower expression of IFNAR1 on myeloid
317 cells, including monocytes (**Figure 3A, B**). *Ifnar1*$^{fl/fl}$ *Lyz2-Cre* mice showed increased tumor
318 growth following STING agonist treatment compared to ADU-S100 *Ifnar1*$^{fl/fl}$ littermate controls
319 (**Figure 3C**). These data suggest that IFN-I responses in infMCs are required for optimal tumor
320 control in the presence of STING agonists.
321

322 To more directly test if infMCs were driven by IFN-I, we analysed responses to STING agonist
323 therapy in mixed bone marrow chimeras in which the hematopoietic cells were derived from a 1:1
324 mix of *Ifnar1*$^{+/+}$ or *Ifnar1*$^{-/-}$ bone marrow cells (**Figure 3D**). The increase in numbers of cDC1,
325 cDC2 and Ly6C^{hi} MCs in the LN at day 1 following STING agonist therapy was largely
326 independent of intrinsic IFN-I signaling (**Figure 3E**). However, upregulation of inflammatory
327 markers CD64 and MAR-1 by Ly6C^{hi} MCs in the LN and tumor was mainly restricted to the wild-
328 type compartment of the chimeric mice (**Figure 3F-H**). These data indicate that intrinsic IFN-I
329 signaling drives an inflammatory phenotype in Ly6C^{hi} MCs but is not required for MC migration
330 to the LN during STING agonist therapy.
331
332 To define how intrinsic IFN-I signalling downstream of intratumoral STING agonist treatment
333 alters the transcriptional state of myeloid cells, CITE-sequencing was performed on immune cells
334 derived from the LNs and tumors of *Ifnar1* mixed bone marrow chimeric mice treated with ADU-
335 S100 or vehicle control (**Figure 4A**). Mice were reconstituted with a 1:1 mix of *Ifnar1*$^{+/+}$ and
336 *Ifnar1*$^{-/-}$ bone marrow cells, and chimerism in the blood was confirmed after 90 days later (**Figure**
337 **S3A, B**). At 12 days following tumor inoculation, mice were treated with ADU-S100 or vehicle
338 and LNs and tumors were harvested 1 day and 2 days post-treatment, respectively. To enrich for
339 myeloid cells, CD3-CD19-CD11b^{+} and/or MHCII^{+} cells were sorted from the LN. Because the
340 tumors are already enriched for myeloid cells, total CD45^{+} cells were sorted from tumors (**Figure**
341 **S3C).** Here, DNA-barcoded antibodies were used to trace the treatment group (vehicle or ADU-
342 S100) and the genotype (*Ifnar1*$^{+/+}$ or *Ifnar1*$^{-/-}$) of each single cell based on the sequencing data
343 (**Figure S3D, E**). After quality filtering, 12, 078 and 3001 cells from the LN and tumor,
344 respectively, remained for downstream analysis (**Figure S3F**). As expected, cells assigned as

345 *Ifnar1*$^{-/-}$ cells expressed very low levels of ISGs compared to *Ifnar1*$^{+/+}$, and ISG expression levels
346 were higher in cells derived from the ADU-S100-treated group compared to vehicle, validating
347 the demultiplexing strategy (**Figure S3G**).
348
349 Clusters of monocytes/macrophages (MC/MP) (CD88/*C5ar1*, CD11b/*Itgam*), cDC1 (XCR1/*Xcr1*,
350 CD26/*Dpp4*) and cDC2 (CD172/*Sirpa*, CD26/*Dpp4*) were identified in the LN and tumor (**Figure**
351 **4B-C**). LN cDCs also expressed high levels of *Ccr7*, as opposed to monocytes, which expressed
352 *Ccr2* and *Ccr5* (**Figure 4B-C**). Each cell type could be further subdivided into subclusters that
353 represent different transcriptional states. Clusters MC_1, cDC1_1 and cDC2_1 in the LN and
354 cluster MC/MF_1 in the tumor were almost exclusively derived from the *Ifnar1*$^{+/+}$ compartment
355 of the STING agonist treated chimeric mice (**Figure 4D**). These clusters shared a common IFN-I
356 gene signature with high expression of interferon signaling genes (ISGs) including *Isg15*, *Isg20*,
357 *Irf7*, *Ifit1*, *Ifi35* and *Bst2* (**Figure 4E-F**). The proportion of MC/MPs with this inflammatory
358 signature was substantially higher in the STING agonist-treated mice compared to controls
359 (**Figure 4G**). Moreover, this state was entirely dependent on intrinsic IFN-I signalling as no *Ifnar1*$^{-}$
360 $^{/-}$ cells were found in these clusters (**Figure 4G**). Because clusters MC_1, cDC1_1 and cDC2_1 in
361 the LN and MC/MP_1 in the tumor are driven by IFN-Is, we will refer to them as infMCs, infDC1
362 and infDC2.
363
364 In the LN and tumor, cells in cluster MC_2 were almost uniquely derived from the *Ifnar1*$^{-/-}$
365 compartment of STING agonist-treated mice, suggesting this state is induced by STING agonist
366 therapy in the absence of intrinsic IFN-I signalling (**Figure 4D**). Cells from clusters MC/MP_3
367 and MC/MP_4 in the tumor were derived from both treatment groups and genotypes, indicating

368 these states are not driven by STING agonist therapy or IFN-I signaling (**Figure 4D**). Cluster
369 MC/MP_4 expressed genes associated with pro-tumorigenic TAMs such as *Vegfa*, *Arg1* and
370 *Cd274* (**Figure 4H**). Pathways associated with cells in tumor cluster MC/MP_4 include
371 "Angiogenesis" and "TGF-β production", suggesting they play a pro-tumorigenic role (**Figure 4I**).
372 The proportion of MC/MP4s was reduced upon STING agonist therapy in an IFN-I-dependent
373 manner (**Figure 4G**). LN and tumor monocyte derived cells also showed IFNAR-1 dependent
374 increases in MHC I genes, along with TAP and proteasome genes (**Figure 4J**). Taken together,
375 these data show that intrinsic IFN-I signaling reduces pro-tumorigenic gene signatures while
376 enhancing genes associated with antigen presentation and inflammatory cytokine production in
377 monocyte-derived cells.
378
379 *InfMCs have a unique inflammatory gene signature compared to infDCs*
380 Inflammatory gene signatures of infMCs, infDC1 and infDC2 were determined by differential
381 gene expression analysis between inflammatory and non-inflammatory subclusters. A core set of
382 214 inflammatory genes were shared between infMCs, infDC1 and infDC2 (**Figure 5A**). These
383 included common ISGs such as *Isg15*, *Isg20* and *Ifit1*. Inflammatory genes that were more highly
384 expressed by infMCs included the cytokine *Il18*, the chemokines *Ccl2*, *Cxcl9* and *Cxcl10*, cell
385 surface molecules *Fcgr1* and *Ly6c2*. In contrast, infDCs expressed higher levels of *Il15*, *Cd70*,
386 *CD86* and *Cd274* (**Figure 5B**). Regulatory network inference predicted that the inflammatory
387 programs in infMCs, infDC1 and infDC2 are driven by different transcriptional regulators
388 downstream of IFN-I signaling. While infMCs were driven by ISGF3 (*Stat1*, *Stat2* and *Irf9*), *Irf5*
389 and *Irf7*, infDCs were predominantly driven by NF-κB family members (*Nfkb2*, *Rel*, *Relb*), *Stat3*,
390 *Stat4* and *Klf6* (**Figure 5C**).

391 By comparing the changes in gene expression between monocytes and macrophages from vehicle
392 and STING-agonist treated mice within the *Ifnar1*$^{+/+}$ and *Ifnar1*$^{-/-}$ compartments, we identified a
393 set of genes that were upregulated upon STING agonist therapy in both the *Ifnar1*$^{+/+}$ and *Ifnar1*$^{-/-}$
394 compartments (**Figure S4**). These included genes involved in the complement system (*C1qa,*
395 *C1qb, C1qc*, *C3ar1*), genes associated with lysosomes including cathepsins (*Ctsb, Ctsc, Ctsd, Ctsl*)
396 and *Lamp1*, as well as genes encoding for the transcription factors *Fosb* and *Maf* (**Figure S4**).
397

398 *Il18 is induced by IFN-I signalling in monocytic lineage cells and is important for the anti-tumor*
399 *response to STING agonists*

400 Receptor-ligand interactions between infMCs and CD8^{+} T cells or NK cells were predicted using
401 NicheNet (28). IL-18 – IL-18R1 interaction was the top predicted interaction between infMCs and
402 CD8^{+} T cells or NK cells (**Figure 6A**). *Il18* expression was specifically upregulated by infMCs
403 and not by infDC1 or infDC2 (**Figure 6A**). IL-18R1 was highly expressed on both tumor-specific
404 CD8^{+} T cells and NK cells in the lymph node and tumor and was upregulated on tumor-specific
405 CD8^{+} T cells upon STING agonist therapy (**Figure 6B-D).** Accordingly, blockade of IL-18 using
406 a neutralizing antibody led to impaired tumor control in mice treated with ADU-S100 (**Figure 6E-**
407 **F**), in line with previous studies that show that activation of the IL-18-IL-18R pathway promotes
408 CD8^{+} T cell and NK cell responses against tumors (36, 37). To determine the contribution of
409 monocyte derived IL-18 to tumor control, we compared the effect of blocking IL-18 with anti-IL-
410 18 antibody in *Ccr2*$^{+/+}$ or *Ccr2*$^{-/-}$ mice (**Figure 6G**). Whereas anti-IL-18 increased tumor growth
411 in WT mice, tumor growth was not impacted by anti-IL-18 in CCR2$^{-/-}$ mice consistent with a role
412 for infMC in provision of IL-18. In addition, we found that blockade of IL-18 in STING agonist
413 treated mice impaired IFN-γ production by tumor Ag-specific CD8 T cells in the LN (Figure 6H-

414 J). These data support a role for monocyte-derived IL-18 in increasing CD8 T cell production of

415 IFN-γ in the dLN, resulting in increased tumor control during STING agonist therapy.

416

417

418 **DISCUSSION**

419 MCs often acquire pro-tumorigenic features in the TME in response to factors such as hypoxia and
420 fibrosis. Therefore, therapeutic strategies have aimed at either depleting these populations or
421 reprogramming them towards more pro-immunogenic states (38). The latter approach may be
422 preferable, as it takes advantage of the anti-tumorigenic features of MCs that are non-redundant
423 with that of other immune cells. STING agonist treatment promotes recruitment of MCs, and the
424 IFN-I production induced by STING agonists drives intrinsic phenotypical, transcriptional, and
425 functional changes in the MC, associated with tumor control.

426

427 We show here that *Ccr2*$^{-/-}$ mice have impaired responses to STING agonist therapy compared to
428 *Ccr2*$^{+/+}$ littermates. CCR2 is required for monocyte egress from the bone marrow, and *Ccr2*$^{-/-}$ mice
429 lack circulating monocytes (33, 34). Although we cannot exclude that *Ccr2*$^{-/-}$ mice might also have
430 defects in the CCR2-dependent migration of other cell populations, the finding that CCR2-
431 deficiency did not impact overall numbers of cDC1 or cDC2, is consistent with monocytes playing
432 a role in STING agonist therapy. Previous studies have reported reduced response to STING
433 agonists in cancer models when mice are treated with chlodronate liposomes (23, 25), which
434 deplete phagocytic cells including macrophages and MCs. Our results complement these studies
435 by suggesting a more specific role of CCR2-dependent MCs, as opposed to tissue macrophages,
436 during STING agonist therapy of cancer and by investigating the intrinsic role of IFN-I signaling
437 in these cells.

438

439 Our experiments using *Ifnar1*$^{fl/fl}$ *Lyz2-Cre* mice indicate that intrinsic IFN-I signaling in *Lyz2*$^{+}$ cells
440 contribute to tumor control in the presence of STING agonists. *Lyz2*-cre is expected to delete

441 floxed genes in approximately 40-50% of blood monocytes with less than 10% deletion in cDCs
442 (39). Accordingly, we observed a significant loss of cell surface IFNAR1 expression on tumor-
443 infiltrating Ly6C^{hi} MCs in *Ifnar1$^{fl/fl}$ Lyz2-Cre* compared to *Ifnar1$^{fl/fl}$* controls. This loss of IFNAR
444 expression was sufficient to significantly reduce cell surface expression of the IFN-I regulated
445 protein CD64 on these cells, validating that this mouse model is relevant to study the role of IFN-
446 I responses in Ly6C^{hi} MCs. While we cannot exclude that IFN-Is in other *Lyz2^{+}* cells such as
447 neutrophils might also contribute to the response to STING agonist therapy, these data combined
448 with the experiments using *Ccr2$^{-/-}$* mice are compatible with a role for IFN-I signaling in
449 monocytes during STING agonist therapy of cancer.
450
451 Some studies have shown a role for monocytes as a source of STING induced IFN-I. For example,
452 Lam et al showed that microbiota-derived STING agonists induced by a high fat diet induced IFN-
453 I production by tumor monocytes to promote DC-NK cell crosstalk (40). Monocytes were also
454 recently found to be the main source of IFN-I after radiation therapy of mice (26), whereas another
455 recent study showed that tumors are the major source of STING-dependent IFN-I in mouse and
456 human cancers (41). We did not observe *Ifn* production by monocytes in our RNA-sequencing
457 data at day 2 post-treatment, albeit we did not further pursue the source of IFN-I in our model.
458
459 A recent study by Tadepalli et al. used depletion of CCR2 positive cells during radiation therapy
460 of mouse tumors to implicate monocytes in CD8 T cell responses and tumor control in a model in
461 which STING is important for the effects of radiation induced tumor control (26). Conversely,
462 Nicolai et al. used IFNAR1 CD11c-cre mice to show that IFN-I responses in cDCs are required
463 for NK-cell mediated tumor control during STING agonist therapy (21). Our findings are

464 complementary to these previous studies on the role of STING during tumor therapy because they
465 highlight the role of CCR2-dependent cells and intrinsic IFN-I signaling in MCs following
466 intratumoral delivery of STING agonists (18, 21, 26, 40, 41).
467
468 Using mixed bone marrow chimeric mice, in which half the hematopoietic cells lack IFNAR1,
469 combined with flow cytometry and CITE-sequencing, we showed that intrinsic IFN-I signaling in
470 monocytic lineage cells drives an inflammatory phenotype characterized by positive staining for
471 CD64 and FcεR1 (MAR-1), akin to infMCs observed in models of acute viral infection (4, 5).
472 Transcriptionally, infMCs express high levels of common ISGs, as well as inflammatory cytokines
473 (*Il15*, *Il18*) and chemokines (*Ccl2, Cxcl9, Cxcl10*). This state is also entirely dependent on intrinsic
474 IFN-I signaling, as *Ifnar1*$^{-/-}$ cells within the same mice do not adopt this transcriptional state,
475 despite exposure to the same environmental cues. Although STING agonists can also induce other
476 cytokines such as TNF and IL-6 (42), the monocyte response is heavily weighted toward IFNAR
477 signaling with only a handful of IFNAR-independent STING induced genes observed (Fig S4).
478 In contrast, the IFN gene signature in DC1 and 2, while present, is weaker than that of monocytes
479 (Figure 4E). Inflammatory DC1, DC2 and infMC shared a core of 214 inflammatory genes.
480 However, analysis of the single cell data by single-cell regulatory network inference analysis
481 suggested while infMCs were driven by ISGF3 (*Stat1*, *Stat2* and *Irf9*), *Irf5* and *Irf7*, infDCs were
482 predominantly driven by NF-κB family members (*Nfkb2*, *Rel*, *Relb*), *Stat3*, *Stat4* and *Klf6,* which
483 is consistent with other cytokines such as TNF and IL-6 also playing a role. Although not further
484 investigated here, this likely reflects the distinct epigenetic and transcriptional state of the different
485 cell types, leading to distinct outcomes.

486 Skewing of monocyte and macrophage populations towards a more pro-inflammatory phenotype
487 during STING agonist therapy was previously reported (23,25), but whether this was driven by
488 intrinsic IFN-I responses had not been tested until now. In line with the study by Xu et al. (23) ,
489 we also find a loss of TAMs with a pro-tumorigenic transcriptional profile upon STING agonist
490 treatment. Interestingly, we report that the lack of this population in STING agonist treated tumors
491 is dependent on intrinsic IFN-I signaling in monocytes, which to our knowledge had not been
492 shown previously. Although we did not formally confirm the loss of TAM markers at the protein
493 level, our findings are consistent with a recent study showing that intrinsic IFNAR1 signaling
494 prevents the acquisition of immune suppressive features by myeloid-derived suppressor cells (43).
495
496 Based on CD64 and FcεR1 (MAR-1) staining, the inflammatory state of monocytic lineage cells
497 in the LN and tumors was transient, peaking at day 1-2 and returning to baseline by day 5 post-
498 ADU-S100 treatment. Monocytic lineage cells might re-acquire a pro-tumorigenic profile in
499 absence of sustained IFN-I signaling. In a breast cancer model, depletion of TAMs with liposome
500 clodronate during the first week of treatment with CAR-T cells and the STING agonist DMXAA
501 reduced tumor control (23). However, depleting TAMs at later time points helped sustain tumor
502 regression, indicating that TAMs reacquired a suppressive profile over time (23). In this case, an
503 alternative approach to cell depletion could be the use of fractionated treatment regimens where
504 STING agonists are given every 2-3 days, as this might sustain inflammatory states and prevent
505 the resurgence of pro-tumorigenic TAMs.
506
507 Although cDC1 are specialized in the cross-presentation of exogenous antigens, other APC
508 populations including monocytes, have been reported to acquire the ability to cross-prime $CD8^+$ T

509 cells if appropriately stimulated (8, 44-47). However, the idea that infMCs can migrate to the LN
510 and effectively cross-prime $CD8^+$ T cells has recently been challenged (29, 31). The
511 characterization of a population of bona-fide cDC2s that express CD64 and stain positive for
512 MAR-1 (infDC2s) suggested that the observed migration and priming ability of infMCs might
513 have been attributable to contaminating cDCs. To accurately delineate infMCs from infDC2s in
514 mice, it is now recommended to use CD26 and CD88 (29). Here, we report that $CD26^-CD88^+$
515 $Ly6C^{hi}$ MCs effectively take up tumor proteins and carry them to the LNs in response to intra-
516 tumoral STING agonist administration. These cells were phenotypically and transcriptionally
517 distinct from $CD26^+CD88^-$ infDCs, and expressed conventional monocyte genes such as *Csf1r*,
518 *Ccr2*, *Itgam* and *Plac8*. A possible explanation for these conflicting findings is that we did not pre-
519 gate on $MHCII^{hi}$ cells in our analyses of infMCs. As infMCs in the LN express significantly lower
520 levels of MHCII than cDCs, pre-gating on $MHCII^{hi}$ cells might exclude them from the analysis.
521
522 Recently, CCR5 has been implicated in trafficking of monocytes to LNs (32). Consistently, we
523 observed CCR5 protein expression on the monocytes. Moreover, *Ccr5* was identified as a
524 monocyte but not DC expressed gene in the CITE-seq data, and the CCR5 antagonist maraviroc
525 substantially reduced the trafficking of monocytes from the tumor to the dLN. We also provided
526 evidence that MC in the LN substantially increase IFN-γ production by CD8 T cells through
527 provision of IL-18, suggesting that the trafficking of monocytes to the LN is important in local T
528 cell responses. Although not formally tested here, the presumption is that these cells then migrate
529 back to the tumor to carry out their effector function. Indeed, it has been suggested that the dLN
530 provides an important reservoir of differentiated T cells, protected from the inhibitory environment

531 of the tumor, thus the delivery to the LN of tumor and IL-18 by monocytes may be relevant to the
532 activation of T cells and tumor control (48).
533
534 Our data also showed that STING agonists induce immunological control of tumors at least in
535 part through increased IL-18 production by monocytes. *Il18* was expressed by infMCs which have
536 responded to IFN-I in the tumor and LN after STING agonist therapy. This is in line with previous
537 studies demonstrating that IL-18 is transcriptionally regulated by STING and/or IFN-I signaling
538 (49, 50). We confirmed the biological relevance of IL-18 induction in monocytes, by showing that
539 in vivo neutralization of IL-18 reduced the efficacy of STING agonists in driving tumor control in
540 *Ccr2*$^{+/+}$ but not *Ccr2*$^{-/-}$ mice. Of note, IFN-I dependent production of IL-18 by infMCs is also
541 important for immune responses to viral, parasitic, or bacterial infections (6, 7). While *Il18* and
542 intracellular IL-18 levels are upregulated in MCs upon exposure to IFN-Is, IL-18 requires
543 proteolytic cleavage downstream of inflammasome activation to be secreted. There is evidence
544 that the cGAS-STING-IFN-I axis activates the inflammasome in human and mouse MCs (51-53).
545
546 We also observed strong IFNAR1-dependent increases in MHC I and genes associated with Ag
547 presentation in the CITE-seq data and we observed increased MHC I protein expression on the
548 infMC in response to STING agonist therapy, consistent with increased peptide loading. However,
549 *Ccr2*$^{-/-}$ mice which lack infMC, did not show impairment in the initial proliferation of adoptively
550 transferred OT-I T cells compared to WT mice, arguing that infMCs are not significantly
551 contributing to T cell priming in this model. These findings are consistent with the observation
552 Batf3^{+} DCs are important for T cell priming during STING agonist therapy of cancer (54). In viral
553 infection models, signals from monocyte-derived cells promote the post priming accumulation of

554 T cells, with no detectable impact on initial cell proliferation over the first 5 days (4, 55). It is
555 possible that low level of Ag presentation by the monocytes, while insufficient for priming CD8
556 T cells, could contribute to the interaction of the IL-18-producing monocytes with primed T cells
557 in the LN, to augment effector function.
558
559 In conclusion, we have shown that intra-tumoral STING agonist therapy mediates at least part of
560 its effects through infMCs. Mechanistically, STING agonists increased IFN-I signaling in
561 monocytes, driving a unique inflammatory state that includes production of IL-18, which was
562 important for CD8 T cell production of IFN-γ in the dLN, and for tumor control. Taken together,
563 these findings highlight the importance of infMCs in STING agonist therapy of cancer. Monitoring
564 STING agonist therapy in humans for induction of infMCs and IL-18 could help optimize such
565 therapies.
566
567 **Acknowledgements:** The authors thank Birinder Ghumman for technical assistance; Nathalie
568 Simard and Janine Charron for assistance with fluorescence-activated cell sorting; Dr Slava
569 Epelman and Rysa Zaman for breeding *Ifnar1*$^{fl/fl}$ *Lyz2-Cre* mice; Dr Jean Gariépy for sharing the
570 MC-38 cell line, and Drs. Sonya MacParland and Arthur Mortha for critical reading of the
571 manuscript.
572
573
574
575

576 **References:**

577 1. DeNardo, D. G., and B. Ruffell. 2019. Macrophages as regulators of tumour immunity
578 and immunotherapy. *Nature Reviews Immunology* 19: 369-382.
579 2. Ugel, S., S. Cane, F. De Sanctis, and V. Bronte. 2021. Monocytes in the Tumor
580 Microenvironment. *Annu Rev Pathol* 16: 93-122.
581 3. Olingy, C. E., H. Q. Dinh, and C. C. Hedrick. 2019. Monocyte heterogeneity and
582 functions in cancer. *J Leukoc Biol* 106: 309-322.
583 4. Chang, Y. H., K. C. Wang, K. L. Chu, D. L. Clouthier, A. T. Tran, M. S. Torres Perez, A.
584 C. Zhou, A. A. Abdul-Sater, and T. H. Watts. 2017. Dichotomous Expression of TNF
585 Superfamily Ligands on Antigen-Presenting Cells Controls Post-priming Anti-viral
586 CD4(+) T Cell Immunity. *Immunity* 47: 943-958 e949.
587 5. Chu, K. L., N. V. Batista, K. C. Wang, A. C. Zhou, and T. H. Watts. 2019. GITRL on
588 inflammatory antigen presenting cells in the lung parenchyma provides signal 4 for T-cell
589 accumulation and tissue-resident memory T-cell formation. *Mucosal Immunol* 12: 363-
590 377.
591 6. Lee, A. J., B. Chen, M. V. Chew, N. G. Barra, M. M. Shenouda, T. Nham, N. van
592 Rooijen, M. Jordana, K. L. Mossman, R. D. Schreiber, M. Mack, and A. A. Ashkar.
593 2017. Inflammatory monocytes require type I interferon receptor signaling to activate NK
594 cells via IL-18 during a mucosal viral infection. *J Exp Med* 214: 1153-1167.
595 7. Soudja, S. M., A. L. Ruiz, J. C. Marie, and G. Lauvau. 2012. Inflammatory monocytes
596 activate memory CD8(+) T and innate NK lymphocytes independent of cognate antigen
597 during microbial pathogen invasion. *Immunity* 37: 549-562.

598 8. Bedford, J. G., M. Heinlein, A. L. Garnham, T. H. O. Nguyen, T. Loudovaris, C. Ge, S. I.
599 Mannering, M. Elliott, S. G. Tangye, K. Kedzierska, D. H. D. Gray, W. R. Heath, and L.
600 M. Wakim. 2020. Unresponsiveness to inhaled antigen is governed by conventional
601 dendritic cells and overridden during infection by monocytes. *Sci Immunol* 5. eabb5439
602 9. Chu, K. L., N. V. Batista, M. Girard, and T. H. Watts. 2020. Monocyte-Derived Cells in
603 Tissue-Resident Memory T Cell Formation. *J Immunol* 204: 477-485.
604 10. Ishikawa, H., and G. N. Barber. 2008. STING is an endoplasmic reticulum adaptor that
605 facilitates innate immune signalling. *Nature* 455: 674-678.
606 11. Ishikawa, H., Z. Ma, and G. N. Barber. 2009. STING regulates intracellular DNA-
607 mediated, type I interferon-dependent innate immunity. *Nature* 461: 788-792.
608 12. Sun, L., J. Wu, F. Du, X. Chen, and Z. J. Chen. 2013. Cyclic GMP-AMP synthase is a
609 cytosolic DNA sensor that activates the type I interferon pathway. *Science* 339: 786-791.
610 13. Wu, J., L. Sun, X. Chen, F. Du, H. Shi, C. Chen, and Z. J. Chen. 2013. Cyclic GMP-
611 AMP is an endogenous second messenger in innate immune signaling by cytosolic DNA.
612 *Science* 339: 826-830.
613 14. Woo, S. R., M. B. Fuertes, L. Corrales, S. Spranger, M. J. Furdyna, M. Y. Leung, R.
614 Duggan, Y. Wang, G. N. Barber, K. A. Fitzgerald, M. L. Alegre, and T. F. Gajewski.
615 2014. STING-dependent cytosolic DNA sensing mediates innate immune recognition of
616 immunogenic tumors. *Immunity* 41: 830-842.
617 15. Deng, L., H. Liang, M. Xu, X. Yang, B. Burnette, A. Arina, X. D. Li, H. Mauceri, M.
618 Beckett, T. Darga, X. Huang, T. F. Gajewski, Z. J. Chen, Y. X. Fu, and R. R.
619 Weichselbaum. 2014. STING-Dependent Cytosolic DNA Sensing Promotes Radiation-

620 Induced Type I Interferon-Dependent Antitumor Immunity in Immunogenic Tumors.
621 *Immunity* 41: 843-852.
622 16. Corrales, L., L. H. Glickman, S. M. McWhirter, D. B. Kanne, K. E. Sivick, G. E.
623 Katibah, S. R. Woo, E. Lemmens, T. Banda, J. J. Leong, K. Metchette, T. W. Dubensky,
624 Jr., and T. F. Gajewski. 2015. Direct Activation of STING in the Tumor
625 Microenvironment Leads to Potent and Systemic Tumor Regression and Immunity. *Cell*
626 *Rep* 11: 1018-1030.
627 17. Fu, J., D. B. Kanne, M. Leong, L. H. Glickman, S. M. McWhirter, E. Lemmens, K.
628 Mechette, J. J. Leong, P. Lauer, W. Liu, K. E. Sivick, Q. Zeng, K. C. Soares, L. Zheng,
629 D. A. Portnoy, J. J. Woodward, D. M. Pardoll, T. W. Dubensky, Jr., and Y. Kim. 2015.
630 STING agonist formulated cancer vaccines can cure established tumors resistant to PD-1
631 blockade. *Sci Transl Med* 7: 283ra252.
632 18. Sivick, K. E., A. L. Desbien, L. H. Glickman, G. L. Reiner, L. Corrales, N. H. Surh, T. E.
633 Hudson, U. T. Vu, B. J. Francica, T. Banda, G. E. Katibah, D. B. Kanne, J. J. Leong, K.
634 Metchette, J. R. Bruml, C. O. Ndubaku, J. M. McKenna, Y. Feng, L. Zheng, S. L.
635 Bender, C. Y. Cho, M. L. Leong, A. van Elsas, T. W. Dubensky, Jr., and S. M.
636 McWhirter. 2018. Magnitude of Therapeutic STING Activation Determines CD8(+) T
637 Cell-Mediated Anti-tumor Immunity. *Cell Rep* 25: 3074-3085 e3075.
638 19. Chin, E. N., C. Yu, V. F. Vartabedian, Y. Jia, M. Kumar, A. M. Gamo, W. Vernier, S. H.
639 Ali, M. Kissai, D. C. Lazar, N. Nguyen, L. E. Pereira, B. Benish, A. K. Woods, S. B.
640 Joseph, A. Chu, K. A. Johnson, P. N. Sander, F. Martinez-Pena, E. N. Hampton, T. S.
641 Young, D. W. Wolan, A. K. Chatterjee, P. G. Schultz, H. M. Petrassi, J. R. Teijaro, and

642 L. L. Lairson. 2020. Antitumor activity of a systemic STING-activating non-nucleotide
643 cGAMP mimetic. *Science* 369: 993-999.
644 20. Pan, B. S., S. A. Perera, J. A. Piesvaux, J. P. Presland, G. K. Schroeder, J. N. Cumming,
645 B. W. Trotter, M. D. Altman, A. V. Buevich, B. Cash, S. Cemerski, W. Chang, Y. Chen,
646 P. J. Dandliker, G. Feng, A. Haidle, T. Henderson, J. Jewell, I. Kariv, I. Knemeyer, J.
647 Kopinja, B. M. Lacey, J. Laskey, C. A. Lesburg, R. Liang, B. J. Long, M. Lu, Y. Ma, E.
648 C. Minnihan, G. O'Donnell, R. Otte, L. Price, L. Rakhilina, B. Sauvagnat, S. Sharma, S.
649 Tyagarajan, H. Woo, D. F. Wyss, S. Xu, D. J. Bennett, and G. H. Addona. 2020. An
650 orally available non-nucleotide STING agonist with antitumor activity. *Science* 369:
651 eaba6098
652 21. Nicolai, C. J., N. Wolf, I. C. Chang, G. Kirn, A. Marcus, C. O. Ndubaku, S. M.
653 McWhirter, and D. H. Raulet. 2020. NK cells mediate clearance of CD8(+) T cell-
654 resistant tumors in response to STING agonists. *Sci Immunol* 5: eaaz2738.
655 22. McAndrews, K. M., S. P. Y. Che, V. S. LeBleu, and R. Kalluri. 2021. Effective delivery
656 of STING agonist using exosomes suppresses tumor growth and enhances anti-tumor
657 immunity. *J Biol Chem* 296: 100523.
658 23. Xu, N., D. C. Palmer, A. C. Robeson, P. Shou, H. Bommiasamy, S. J. Laurie, C. Willis,
659 G. Dotti, B. G. Vincent, N. P. Restifo, and J. S. Serody. 2021. STING agonist promotes
660 CAR T cell trafficking and persistence in breast cancer. *J Exp Med* 218: e20200844
661 24. Gogoi, H., S. Mansouri, and L. Jin. 2020. The Age of Cyclic Dinucleotide Vaccine
662 Adjuvants. *Vaccines (Basel)* 8: 453.
663 25. Ohkuri, T., A. Kosaka, K. Ishibashi, T. Kumai, Y. Hirata, K. Ohara, T. Nagato, K.
664 Oikawa, N. Aoki, Y. Harabuchi, E. Celis, and H. Kobayashi. 2017. Intratumoral

665 administration of cGAMP transiently accumulates potent macrophages for anti-tumor
666 immunity at a mouse tumor site. *Cancer Immunol Immunother* 66: 705-716.
667 26. Tadepalli, S., D. R. Clements, S. Saravanan, R. Arroyo Hornero, A. Lüdtke, B.
668 Blackmore, J. A. Paulo, A. Gottfried-Blackmore, D. Seong, S. Park, L. Chan, B. J.
669 Kopecky, Z. Liu, F. Ginhoux, K. J. Lavine, J. P. Murphy, M. Mack, E. E. Graves, and J.
670 Idoyaga. 2023. Rapid recruitment and IFN-I–mediated activation of monocytes dictate
671 focal radiotherapy efficacy. *Science Immunology* 8: eadd7446.
672 27. Aibar, S., C. B. Gonzalez-Blas, T. Moerman, V. A. Huynh-Thu, H. Imrichova, G.
673 Hulselmans, F. Rambow, J. C. Marine, P. Geurts, J. Aerts, J. van den Oord, Z. K. Atak, J.
674 Wouters, and S. Aerts. 2017. SCENIC: single-cell regulatory network inference and
675 clustering. *Nat Methods* 14: 1083-1086.
676 28. Browaeys, R., W. Saelens, and Y. Saeys. 2020. NicheNet: modeling intercellular
677 communication by linking ligands to target genes. *Nat Methods* 17: 159-162.
678 29. Bosteels, C., K. Neyt, M. Vanheerswynghels, M. J. van Helden, D. Sichien, N. Debeuf,
679 S. De Prijck, V. Bosteels, N. Vandamme, L. Martens, Y. Saeys, E. Louagie, M. Lesage,
680 D. L. Williams, S. C. Tang, J. U. Mayer, F. Ronchese, C. L. Scott, H. Hammad, M.
681 Guilliams, and B. N. Lambrecht. 2020. Inflammatory Type 2 cDCs Acquire Features of
682 cDC1s and Macrophages to Orchestrate Immunity to Respiratory Virus Infection.
683 *Immunity* 52: 1039-1056 e1039.
684 30. Tang, X. Z., J. B. Jung, and C. D. C. Allen. 2019. A case of mistaken identity: The MAR-
685 1 antibody to mouse FcepsilonRIalpha cross-reacts with FcgammaRI and FcgammaRIV.
686 *J Allergy Clin Immunol* 143: 1643-1646 e1646.

687 31. Coillard, A., and E. Segura. 2021. Antigen presentation by mouse monocyte-derived
688 cells: Re-evaluating the concept of monocyte-derived dendritic cells. *Mol Immunol* 135:
689 165-169.
690 32. Rawat, K., A. Tewari, X. Li, A. B. Mara, W. T. King, S. L. Gibbings, C. F. Nnam, F. W.
691 Kolling, B. N. Lambrecht, and C. V. Jakubzick. 2023. CCL5-producing migratory
692 dendritic cells guide CCR5+ monocytes into the draining lymph nodes. *J. Exp. Med.* 220:
693 e20222129.
694 33. Engel, D. R., J. Maurer, A. P. Tittel, C. Weisheit, T. Cavlar, B. Schumak, A. Limmer, N.
695 van Rooijen, C. Trautwein, F. Tacke, and C. Kurts. 2008. CCR2 mediates homeostatic
696 and inflammatory release of Gr1(high) monocytes from the bone marrow, but is
697 dispensable for bladder infiltration in bacterial urinary tract infection. *J Immunol* 181:
698 5579-5586.
699 34. Serbina, N. V., and E. G. Pamer. 2006. Monocyte emigration from bone marrow during
700 bacterial infection requires signals mediated by chemokine receptor CCR2. *Nat.*
701 *Immunol.* 7: 311-317.
702 35. Larkin, B., V. Ilyukha, M. Sorokin, A. Buzdin, E. Vannier, and A. Poltorak. 2017.
703 Cutting Edge: Activation of STING in T Cells Induces Type I IFN Responses and Cell
704 Death. *J Immunol* 199: 397-402.
705 36. Zhou, T., W. Damsky, O. E. Weizman, M. K. McGeary, K. P. Hartmann, C. E. Rosen, S.
706 Fischer, R. Jackson, R. A. Flavell, J. Wang, M. F. Sanmamed, M. W. Bosenberg, and A.
707 M. Ring. 2020. IL-18BP is a secreted immune checkpoint and barrier to IL-18
708 immunotherapy. *Nature* 583: 609-614.

709 37. Hu, B., J. Ren, Y. Luo, B. Keith, R. M. Young, J. Scholler, Y. Zhao, and C. H. June.
710 2017. Augmentation of Antitumor Immunity by Human and Mouse CAR T Cells
711 Secreting IL-18. *Cell Rep* 20: 3025-3033.
712 38. DeNardo, D. G., and B. Ruffell. 2019. Macrophages as regulators of tumour immunity
713 and immunotherapy. *Nat Rev Immunol* 19: 369-382.
714 39. Abram, C. L., G. L. Roberge, Y. Hu, and C. A. Lowell. 2014. Comparative analysis of
715 the efficiency and specificity of myeloid-Cre deleting strains using ROSA-EYFP reporter
716 mice. *J Immunol Methods* 408: 89-100.
717 40. Lam, K. C., R. E. Araya, A. Huang, Q. Chen, M. Di Modica, R. R. Rodrigues, A. Lopes,
718 S. B. Johnson, B. Schwarz, E. Bohrnsen, A. P. Cogdill, C. M. Bosio, J. A. Wargo, M. P.
719 Lee, and R. S. Goldszmid. 2021. Microbiota triggers STING-type I IFN-dependent
720 monocyte reprogramming of the tumor microenvironment. *Cell* 184: 5338-5356 e5321.
721 41. Kwart, D., J. He, S. Srivatsan, C. Lett, J. Golubov, E. M. Oswald, P. Poon, X. Ye, J.
722 Waite, A. G. Zaretsky, S. Haxhinasto, E. Au-Yeung, N. T. Gupta, J. Chiu, C. Adler, S.
723 Cherravuru, E. Malahias, N. Negron, K. Lanza, A. Coppola, M. Ni, H. Song, Y. Wei, G.
724 S. Atwal, L. Macdonald, N. S. Oristian, W. Poueymirou, V. Jankovic, M. Fury, I. Lowy,
725 A. J. Murphy, M. A. Sleeman, B. Wang, and D. Skokos. 2022. Cancer cell-derived type I
726 interferons instruct tumor monocyte polarization. *Cell Reports* 41:111769.
727 42. Zhou, J., Z. Zhuang, J. Li, and Z. Feng. 2023. Significance of the cGAS-STING Pathway
728 in Health and Disease. *Int J Mol Sci* 24: 13316.
729 43. Alicea-Torres, K., E. Sanseviero, J. Gui, J. Chen, F. Veglia, Q. Yu, L. Donthireddy, A.
730 Kossenkov, C. Lin, S. Fu, C. Mulligan, B. Nam, G. Masters, F. Denstman, J. Bennett, N.
731 Hockstein, A. Rynda-Apple, Y. Nefedova, S. Y. Fuchs, and D. I. Gabrilovich. 2021.

732 Immune suppressive activity of myeloid-derived suppressor cells in cancer requires
733 inactivation of the type I interferon pathway. *Nat Commun* 12: 1717.
734 44. Kuhn, S., J. Yang, and F. Ronchese. 2015. Monocyte-Derived Dendritic Cells Are
735 Essential for CD8(+) T Cell Activation and Antitumor Responses After Local
736 Immunotherapy. *Front Immunol* 6: 584.
737 45. Tang-Huau, T. L., P. Gueguen, C. Goudot, M. Durand, M. Bohec, S. Baulande, B.
738 Pasquier, S. Amigorena, and E. Segura. 2018. Human in vivo-generated monocyte-
739 derived dendritic cells and macrophages cross-present antigens through a vacuolar
740 pathway. *Nat Commun* 9: 2570.
741 46. Faure, F., M. Jouve, I. Lebhar-Peguillet, C. Sadaka, F. Sepulveda, O. Lantz, S. Berre, R.
742 Gaudin, S. Sanchez-Ramon, and S. Amigorena. 2018. Blood monocytes sample
743 MelanA/MART1 antigen for long-lasting cross-presentation to CD8(+) T cells after
744 differentiation into dendritic cells. *Int J Cancer* 142: 133-144.
745 47. Duong, E., T. B. Fessenden, E. Lutz, T. Dinter, L. Yim, S. Blatt, A. Bhutkar, K. D.
746 Wittrup, and S. Spranger. 2021. Type I interferon activates MHC class I-dressed
747 CD11b(+) conventional dendritic cells to promote protective anti-tumor CD8(+) T cell
748 immunity. *Immunity* 55: 308-323 e9.
749 48. Delclaux, I., K. S. Ventre, D. Jones, and A. W. Lund. 2024. The tumor-draining lymph
750 node as a reservoir for systemic immune surveillance. *Trends in Cancer* 10: 28-37.
751 49. Zhu, Q., and T. D. Kanneganti. 2017. Cutting Edge: Distinct Regulatory Mechanisms
752 Control Proinflammatory Cytokines IL-18 and IL-1beta. *J Immunol* 198: 4210-4215.
753 50. Ahn, J., S. Son, S. C. Oliveira, and G. N. Barber. 2017. STING-Dependent Signaling
754 Underlies IL-10 Controlled Inflammatory Colitis. *Cell Rep* 21: 3873-3884.

755 51. Wang, W., D. Hu, C. Wu, Y. Feng, A. Li, W. Liu, Y. Wang, K. Chen, M. Tian, F. Xiao,
756 Q. Zhang, M. A. Shereen, W. Chen, P. Pan, P. Wan, K. Wu, and J. Wu. 2020. STING
757 promotes NLRP3 localization in ER and facilitates NLRP3 deubiquitination to activate
758 the inflammasome upon HSV-1 infection. *PLoS Pathog* 16: e1008335.
759 52. Gaidt, M. M., T. S. Ebert, D. Chauhan, K. Ramshorn, F. Pinci, S. Zuber, F. O'Duill, J. L.
760 Schmid-Burgk, F. Hoss, R. Buhmann, G. Wittmann, E. Latz, M. Subklewe, and V.
761 Hornung. 2017. The DNA Inflammasome in Human Myeloid Cells Is Initiated by a
762 STING-Cell Death Program Upstream of NLRP3. *Cell* 171: 1110-1124 e1118.
763 53. Swanson, K. V., R. D. Junkins, C. J. Kurkjian, E. Holley-Guthrie, A. A. Pendse, R. El
764 Morabiti, A. Petrucelli, G. N. Barber, C. A. Benedict, and J. P. Ting. 2017. A
765 noncanonical function of cGAMP in inflammasome priming and activation. *J Exp Med*
766 214: 3611-3626.
767 54. Jneid, B., A. Bochnakian, C. Hoffmann, F. Delisle, E. Djacoto, P. Sirven, J. Denizeau, C.
768 Sedlik, Y. Gerber-Ferder, F. Fiore, R. Akyol, C. Brousse, R. Kramer, I. Walters, S.
769 Carlioz, H. Salmon, B. Malissen, M. Dalod, E. Piaggio, and N. Manel. 2023. Selective
770 STING stimulation in dendritic cells primes antitumor T cell responses. *Sci Immunol* 8:
771 eabn6612.
772 55. Watts, T. H., K. K. M. Yeung, T. Yu, S. Lee, and R. Eshraghisamani. 2025. TNF/TNFR
773 Superfamily Members in Costimulation of T Cell Responses—Revisited. *Annual Review*
774 *of Immunology*. online ahead of print.
775
776
777

778 **Footnotes**

779

780 1. **Funding:** This research was funded by Canadian Cancer Society grant #706759, Canadian
781 Institutes of Health Research (CIHR) grants # FDN-143250, PJ4-185649 and PJT 190128
782 (all to THW) and a CIHR Canada graduate scholarships doctoral award (MG). THW holds
783 the Canada research chair in anti-viral immunity at the University of Toronto

784 2. **Current address:** Department of Microbiology & Immunology, University of California,
785 San Francisco, San Francisco, California, USA.

786 3. **Corresponding author:** Corresponding author: Dr. Tania H. Watts, Department of
787 Immunology, University of Toronto, 1 King's College Circle, Toronto, ON M5S 1A8,
788 Canada. E-mail address: tania.watts@utoronto.ca Tel 416-978-4551

789

790

791 **Figure legends**

792 **Figure 1. InfMCs accumulate in tumors and show CCR5-dependent trafficking to LN**
793 **following STING agonist treatment. (A-H)** STING agonists drive the accumulation of $CD64^+$
794 $MAR\text{-}1^+$ infMCs in the LN and tumor. **(A)** Experimental layout for panels (B-H). Mice were
795 inoculated with 10^6 B16.OVA cells intradermally and given an intratumoral injection of ADU-
796 S100 or vehicle 12 days later. Tumors and draining LNs were harvested for flow cytometric
797 analysis at 0-5 days post-treatment. (**B)** Gating strategy for identification of cDC1
798 ($CD26^+MHCII^{hi}CD11c^+XCR1^+$), cDC2 ($CD26^+MHCII^{hi}CD11c^+CD172^+$), $Ly6C^{hi}$ MCs (CD26-
799 $CD11b^+Ly6G\text{-}Ly6C^+$) and infMCs ($CD26\text{-}CD11b^+Ly6G\text{-}Ly6C^+CD64^+MAR\text{-}1^+$) in the LN and
800 tumor, starting from single, live $CD45^+$ cells. **(C-H)** Number and percentage of cells in the LN (C-
801 E) and tumor (F-H) at indicated time points after treatment with ADU-S100 or vehicle. **(I-K)**
802 InfMCs carry tumor antigens to the LN. **(I)** Experimental layout for panels (J,K). C57BL/6 mice
803 were inoculated with 10^6 B16.OVA.tomato cells intradermally and given ADU-S100 or vehicle 12
804 days later. LNs were collected for flow cytometry on day 2 post-treatment. **(J)** Representative flow
805 plots. **(D)** Tomato signal in LN APC populations depicted as the tomato MFI (left panel), %
806 $tomato^+$ (middle panel) and absolute number of $tomato^+$ cells (right panel). (L) Experimental
807 design for panels (M-N). B16.OVA.tomato tumor-bearing C57BL/6 mice were given 10mg/kg
808 maraviroc or PBS treatment 4 hours prior to ADU-S100 or vehicle treatment. TDLNs were
809 collected for flow cytometry on day 1 post-treatment. (M) Tomato signal in LN $Ly6C^{hi}$ MC
810 population depicted as absolute number of $tomato^+$ cells. (N) CCR5 expression on $Ly6C^{hi}$ MCs,
811 cDC1 and cDC2 in TDLN one day after ADU-S100 treatment. Data are pooled from two or three
812 independent experiments, each with 3-6 mice per group. Unpaired t-test (D,E,G,H), two-way
813 ANOVA (K,M), or one-way ANOVA with Sidak's multiple comparisons test (N) was performed.

814 **Figure 2. InfMCs are required for optimal responses to STING agonist therapy. (A)** Number
815 and percentage of infMCs in B16.OVA tumors of *Ccr2*$^{+/+}$ and *Ccr2*$^{-/-}$ mice two days post-treatment
816 with ADU-S100 or vehicle. **(B-C),** Volume of B16.OVA intradermal tumors (B) or MC-38
817 subcutaneous tumors (C) in *Ccr2*$^{+/+}$ and *Ccr2*$^{-/-}$ mice treated with ADU-S100 or vehicle on days
818 indicated by an arrow. **(D-E),** Ki-67 staining on LN H-2K^{b} SIINFEKL tetramer^{+} CD8^{+} T cells (D)
819 or NK cells (E) three days post-treatment with ADU-S100 or vehicle. Data are representative of
820 two independent experiments. One-way ANOVA (A, D-E), or two-way ANOVA with Sidak's
821 multiple comparisons test (B,C) was performed.
822
823 **Figure 3. Intrinsic IFN-I signaling drives an inflammatory phenotype in Ly6C^{hi} MCs but is**
824 **dispensable for their migration to the LN. (A)** Experimental layout for panels (B,C). *Ifnar1*$^{fl/fl}$
825 and *Ifnar1*$^{fl/fl}$ *Lyz2-Cre* mice were inoculated with B16.OVA tumors and treated with ADU-S100
826 or vehicle 12 days later. **(B)** IFNAR1, CD64 and MAR-1 staining on Ly6C^{hi} MCs from the
827 B16F10.OVA tumors of *Ifnar1*$^{fl/fl}$ and *Ifnar1*$^{fl/fl}$ *Lyz2-Cre* mice on day 5 post-treatment. **(C)**
828 Volume of B16F10.OVA tumors in *Ifnar1*$^{fl/fl}$ and *Ifnar1*$^{fl/fl}$ *Lyz2-Cre* mice treated with ADU-S100
829 on day 11. **(D)** Experimental layout for panels (E-G). Irradiated CD45.1/.2 mice were reconstituted
830 with a 1:1 mixture of CD45.1 *Ifnar1*$^{+/+}$ and CD45.2 *Ifnar1*$^{-/-}$ bone marrow cells. After >90 days
831 reconstitution, mice were inoculated with 10^{6} B16F10.OVA cells intradermally and given ADU-
832 S100 or vehicle intratumorally 12 days later. TDLNs and tumors were collected 1- and 2-days
833 post-treatment, respectively for flow cytometric analysis. **(E)** Absolute numbers of *Ifnar1*$^{+/+}$ and
834 *Ifnar1*$^{-/-}$ cDC1, cDC2 and Ly6C^{hi} MCs in the TDLNs (top) and tumors (bottom) of the mixed bone
835 marrow chimeric mice. **(F)** Percentage of Ly6C^{hi} MCs that express the infMC markers CD64 and
836 MAR-1 in the TDLNs (top) and tumors (bottom) of the mixed bone marrow chimeric mice. **(G)**

837 Mean fluorescent intensity of CD64 and MAR-1 on Ly6C^{hi} MCs in the TDLNs (top) and tumors
838 (bottom) of the mixed bone marrow chimeric mice. Data are pooled from two independent
839 experiments with 3-4 mice each.Unpaired t-test (B), two-way ANOVA with Sidak's multiple
840 comparisons test (C), or One-way ANOVA with Tukey's multiple comparisons test (E-G) was
841 performed.
842
843 **Figure 4. Intrinsic IFN-I signaling drives an inflammatory transcriptional state in LN and**
844 **tumor monocytes.** CITE-sequencing analysis of myeloid cells from the LNs and tumors of *Ifnar1*
845 mixed bone marrow chimeric mice on days 1 and 2 post-treatment with ADU-S100 or vehicle. **(A)**
846 Experimental design. **(B-C)** UMAP of cDC, monocyte and macrophage populations in the LN. (B)
847 and tumor (C). **(D)** Proportion of cells in each cluster derived from each genotype and treatment
848 condition. **(E-F)** UMAP depicting the IFN-I signature score for each cell in the LN (E) and tumor
849 (F). On the right, dotplots depicting the expression of common ISGs across clusters. **(G)**
850 Percentage of total monocytes/macrophages in each group derived from each cluster. **(H)**
851 Heatmaps depicting top DEGs across or tumor monocyte/macrophage clusters. **(I)** Pathway
852 enrichment analysis (g:Profiler, GO biological processes) using DEGs for each tumor
853 monocyte/macrophage cluster (Mono/Mac 1-5). **(J)** Expression of genes involved in antigen
854 processing and presentation via MHC class I in monocyte/macrophages from the LN and tumor of
855 *Ifnar1* mixed bone marrow chimeric mice treated with ADU-S100 or vehicle.
856
857 **Figure 5. InfMCs have a unique inflammatory program compared to infDCs. (A)**
858 Inflammatory signatures for infMCs, infDC1 and infDC2 were calculated and compared in a Venn
859 diagram. **(B)** Heatmaps depicting differential expression of selected inflammatory genes across

860 infAPC populations. **(C)** Heatmap depicting the percentage of cells in each infAPC population in
861 which the indicated regulons are active, as determined by single-cell regulatory network inference
862 analysis.
863
864 **Figure 6. IL-18 is required for optimal tumor control in response to STING agonists. (A)**
865 NicheNet analysis of receptor ligand interactions between infAPC populations and $CD8^+$ T cells
866 or NK cells. **(B)** Gating strategy to identify H-$2K^b$ SIINFEKL $tetramer^+$ $CD8^+$ T cells and NK cells
867 in the LNs starting from live $CD45^+$ cells. **(C-E)** Mice were administered 200 µg anti-IL-18 or
868 control IgG2a intraperitoneally twice: one day before and one day after intra-tumoral
869 administration of ADU-S100 or vehicle control. **(C-D)** Expression of IL-18R1 on LN H-$2K^b$
870 SIINFEKL $tetramer^+$ $CD8^+$ T cells (C) and NK cells (D) 3 days post-treatment with ADU-S100.
871 **(E)** Experimental design for panels (F-G)**. (F)** Volume of B16.OVA tumors in mice treated with
872 anti-IL-18 or IgG2a and ADU-S100. (**G**) Volume of B16.OVA tumors in *Ccr2*$^{+/+}$ and *Ccr2*$^{-/-}$
873 littermate mice treated with anti-IL-18 or IgG2a and ADU-S100. **(H)** Experimental design for
874 panels (I-J) **(I)**. Representative flow cytometry data for IFN-γ production by live CD8 $CD44^{hi}$ T
875 cells in the dLN, day 3 after STING agonist treatment, showing no peptide control, as well as
876 restimulation with Trp-2 peptide, for the anti-IL-18 or isotype control treated mice. **(J)**. Summary
877 of two experiments with 3-4 mice per group per experiment. Data are representative of two
878 independent experiments, each with 4-8 mice per group. One-way ANOVA (C-D), two-way
879 ANOVA with Sidak's multiple comparisons test (F-G), or unpaired t-test (J) was performed.
880

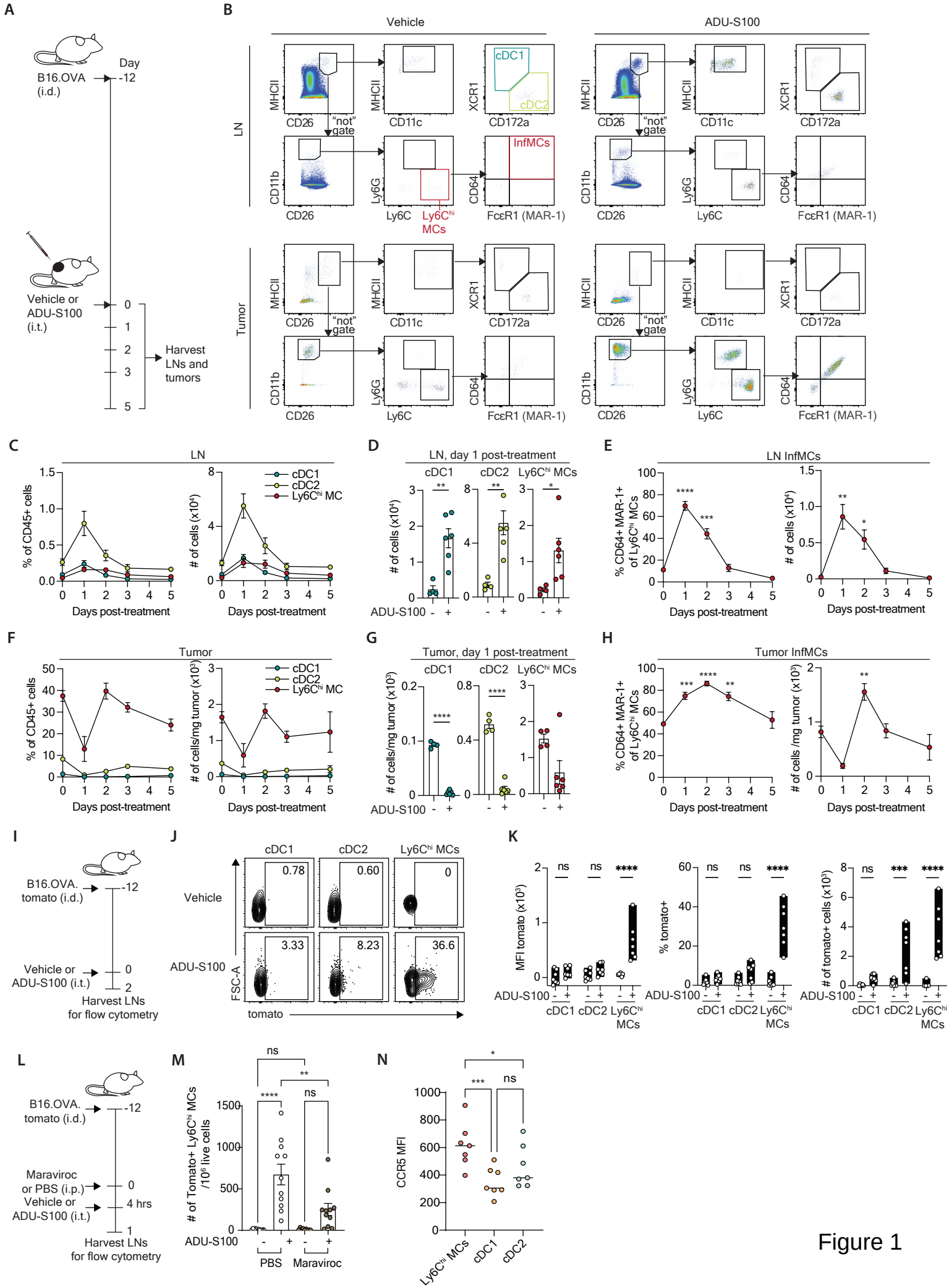
A
B16.OVA (i.d.)
Day -12
Vehicle or ADU-S100 (i.t.)
0
1
2
3
5
Harvest LNs and tumors
B
Vehicle
ADU-S100
LN
Tumor
MHCII
CD26
"not" gate
CD11c
XCR1
CD172a
cDC1
cDC2
CD11b
Ly6G
Ly6C
CD64
FcεR1 (MAR-1)
InfMCs
Ly6C^hi MCs
C
LN
% of CD45+ cells
# of cells (x10^4)
cDC1
cDC2
Ly6C^hi MC
Days post-treatment
D
LN, day 1 post-treatment
cDC1
cDC2
Ly6C^hi MCs
# of cells (x10^4)
ADU-S100
E
LN InfMCs
% CD64+ MAR-1+ of Ly6C^hi MCs
# of cells (x10^4)
F
Tumor
% of CD45+ cells
# of cells/mg tumor (x10^3)
G
Tumor, day 1 post-treatment
H
Tumor InfMCs
I
B16.OVA. tomato (i.d.)
Vehicle or ADU-S100 (i.t.)
Harvest LNs for flow cytometry
J
Vehicle
ADU-S100
FSC-A
tomato
0.78
0.60
0
3.33
8.23
36.6
K
MFI tomato (x10^3)
% tomato+
# of tomato+ cells (x10^3)
ns
****
***
L
B16.OVA. tomato (i.d.)
Maraviroc or PBS (i.p.)
Vehicle or ADU-S100 (i.t.)
4 hrs
Harvest LNs for flow cytometry
M
# of Tomato+ Ly6C^hi MCs /10^6 live cells
PBS
Maraviroc
N
CCR5 MFI
Ly6C^hi MCs
cDC1
cDC2

Figure 1

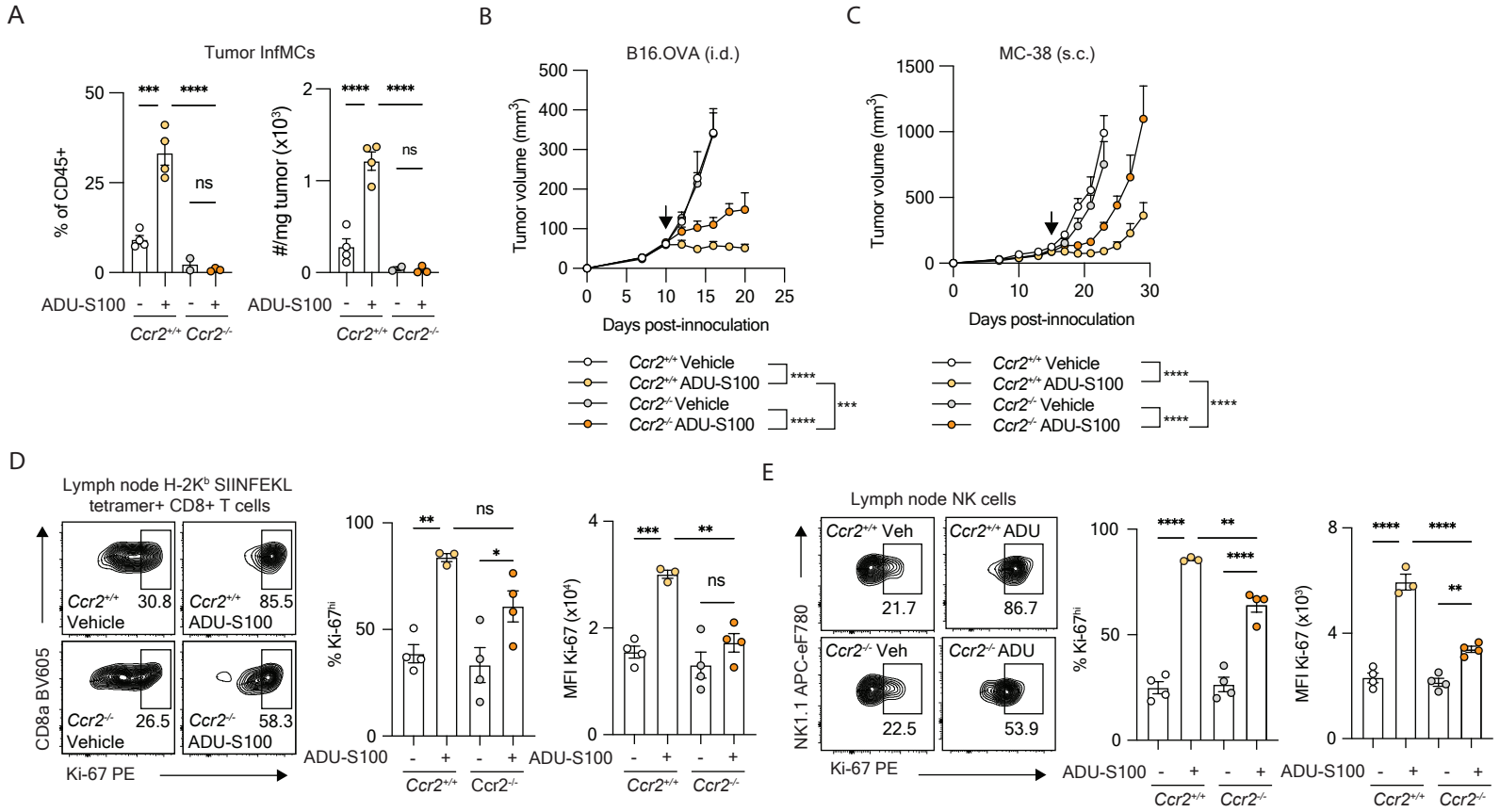
A
Tumor InfMCs
% of CD45+
#/mg tumor (x10³)
ADU-S100
Ccr2+/+ Ccr2-/-
B
B16.OVA (i.d.)
Tumor volume (mm³)
Days post-innoculation
Ccr2+/+ Vehicle
Ccr2+/+ ADU-S100
Ccr2-/- Vehicle
Ccr2-/- ADU-S100
C
MC-38 (s.c.)
D
Lymph node H-2Kᵇ SIINFEKL tetramer+ CD8+ T cells
CD8a BV605
Ki-67 PE
30.8
85.5
26.5
58.3
% Ki-67hi
MFI Ki-67 (x10⁴)
E
Lymph node NK cells
NK1.1 APC-eF780
21.7
86.7
22.5
53.9
MFI Ki-67 (x10³)

Figure 2

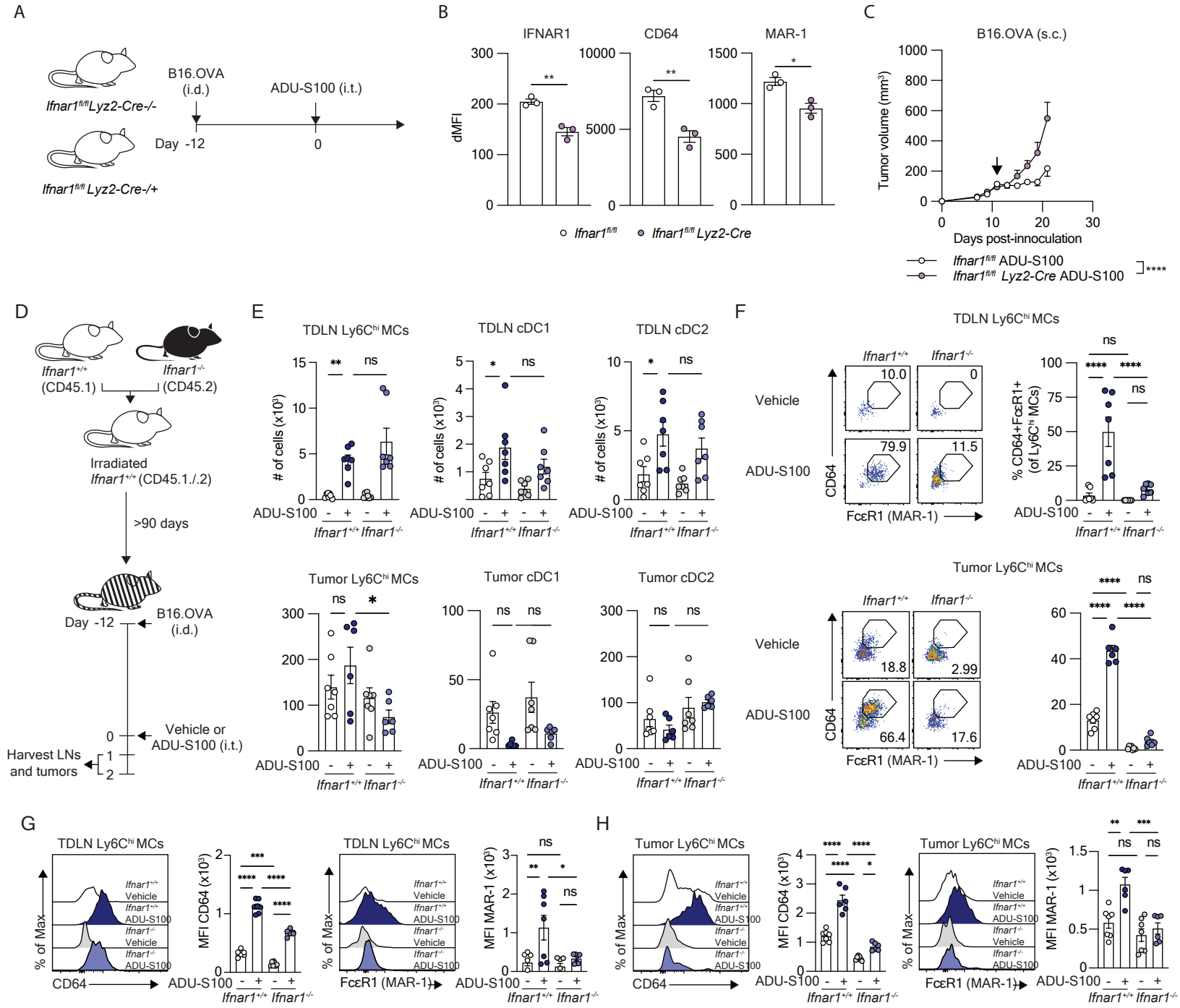
A
Ifnar1fl/flLyz2-Cre-/-
Ifnar1fl/fl Lyz2-Cre-/+
B16.OVA (i.d.)
ADU-S100 (i.t.)
Day -12
0
B
IFNAR1
CD64
MAR-1
dMFI
Ifnar1fl/fl
Ifnar1fl/fl Lyz2-Cre
C
B16.OVA (s.c.)
Tumor volume (mm3)
Days post-innoculation
Ifnar1fl/fl ADU-S100
Ifnar1fl/fl Lyz2-Cre ADU-S100
D
Ifnar1+/+ (CD45.1)
Ifnar1-/- (CD45.2)
Irradiated Ifnar1+/+ (CD45.1./.2)
>90 days
Day -12
B16.OVA (i.d.)
Vehicle or ADU-S100 (i.t.)
Harvest LNs and tumors
E
TDLN Ly6Chi MCs
TDLN cDC1
TDLN cDC2
# of cells (x103)
ADU-S100
Ifnar1+/+ Ifnar1-/-
Tumor Ly6Chi MCs
Tumor cDC1
Tumor cDC2
F
TDLN Ly6Chi MCs
Vehicle
ADU-S100
CD64
FcεR1 (MAR-1)
% CD64+FcεR1+ (of Ly6Chi MCs)
Tumor Ly6Chi MCs
G
TDLN Ly6Chi MCs
% of Max
CD64
MFI CD64 (x103)
FcεR1 (MAR-1)
MFI MAR-1 (x103)
H
Tumor Ly6Chi MCs

Figure 3

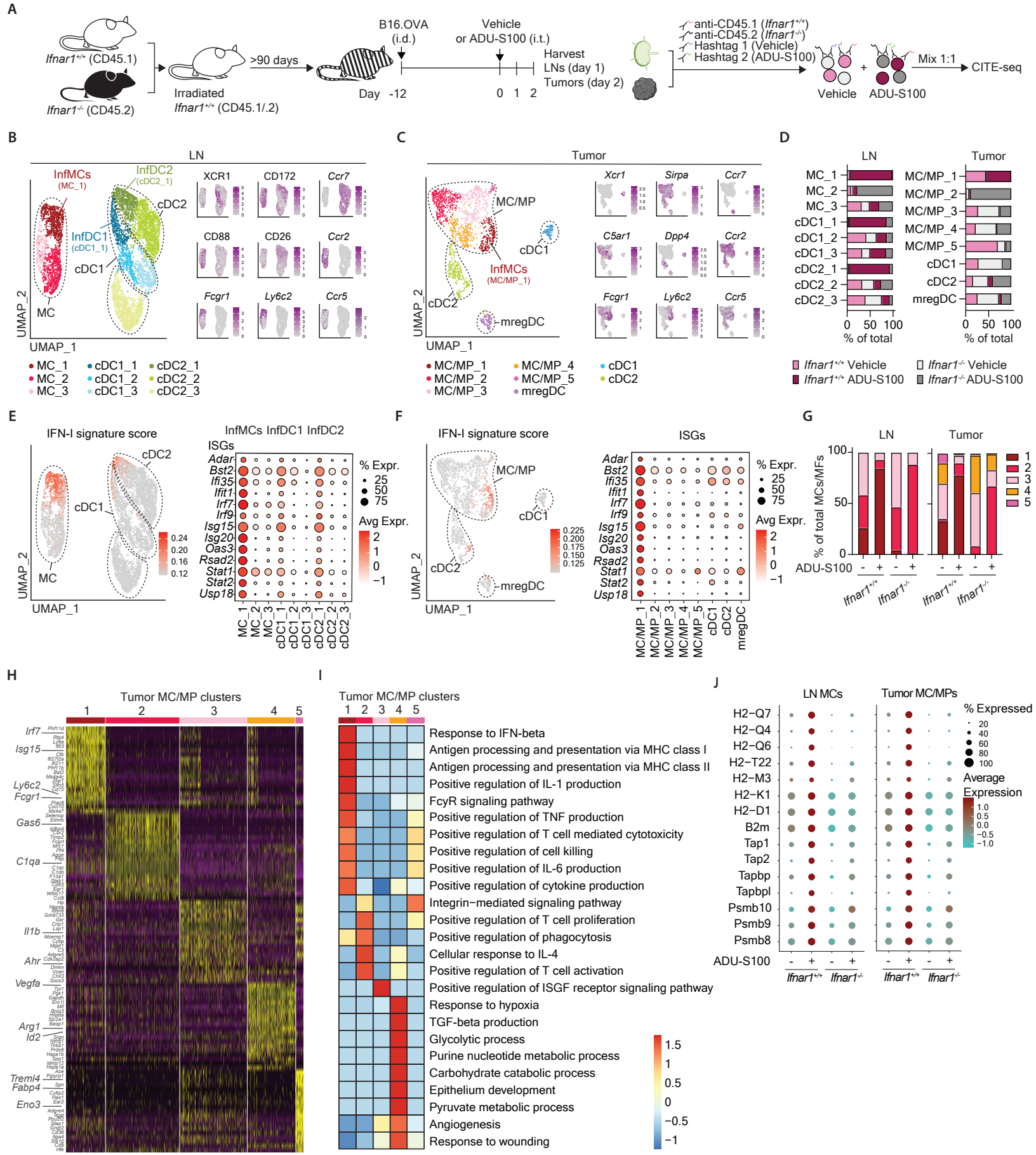
A
Ifnar1+/+ (CD45.1)
Ifnar1-/- (CD45.2)
Irradiated Ifnar1+/+ (CD45.1/.2)
>90 days
B16.OVA (i.d.)
Vehicle or ADU-S100 (i.t.)
Day -12
0 1 2
Harvest
LNs (day 1)
Tumors (day 2)
anti-CD45.1 (Ifnar1+/+)
anti-CD45.2 (Ifnar1-/-)
Hashtag 1 (Vehicle)
Hashtag 2 (ADU-S100)
Vehicle
ADU-S100
Mix 1:1
CITE-seq
B
LN
InfMCs (MC_1)
InfDC2 (cDC2_1)
cDC2
InfDC1 (cDC1_1)
cDC1
MC
UMAP_1
UMAP_2
XCR1
CD172
Ccr7
CD88
CD26
Ccr2
Fcgr1
Ly6c2
Ccr5
MC_1
MC_2
MC_3
cDC1_1
cDC1_2
cDC1_3
cDC2_1
cDC2_2
cDC2_3
C
Tumor
MC/MP
cDC1
InfMCs (MC/MP_1)
cDC2
mregDC
Xcr1
Sirpa
Ccr7
C5ar1
Dpp4
Ccr2
Fcgr1
Ly6c2
Ccr5
MC/MP_1
MC/MP_2
MC/MP_3
MC/MP_4
MC/MP_5
mregDC
cDC1
cDC2
D
LN
Tumor
% of total
Ifnar1+/+ Vehicle
Ifnar1+/+ ADU-S100
Ifnar1-/- Vehicle
Ifnar1-/- ADU-S100
E
IFN-I signature score
ISGs
InfMCs InfDC1 InfDC2
Adar
Bst2
Ifi35
Ifit1
Irf7
Irf9
Isg15
Isg20
Oas3
Rsad2
Stat1
Stat2
Usp18
% Expr.
Avg Expr.
F
IFN-I signature score
ISGs
G
LN
Tumor
% of total MCs/MFs
ADU-S100
Ifnar1+/+
Ifnar1-/-
H
Tumor MC/MP clusters
Irf7
Isg15
Ly6c2
Fcgr1
Gas6
C1qa
Il1b
Ahr
Vegfa
Arg1
Id2
Tremlin4
Fabp4
Eno3
I
Tumor MC/MP clusters
Response to IFN-beta
Antigen processing and presentation via MHC class I
Antigen processing and presentation via MHC class II
Positive regulation of IL-1 production
FcγR signaling pathway
Positive regulation of TNF production
Positive regulation of T cell mediated cytotoxicity
Positive regulation of cell killing
Positive regulation of IL-6 production
Positive regulation of cytokine production
Integrin-mediated signaling pathway
Positive regulation of T cell proliferation
Positive regulation of phagocytosis
Cellular response to IL-4
Positive regulation of T cell activation
Positive regulation of ISGF receptor signaling pathway
Response to hypoxia
TGF-beta production
Glycolytic process
Purine nucleotide metabolic process
Carbohydrate catabolic process
Epithelium development
Pyruvate metabolic process
Angiogenesis
Response to wounding
J
LN MCs
Tumor MC/MPs
H2-Q7
H2-Q4
H2-Q6
H2-T22
H2-M3
H2-K1
H2-D1
B2m
Tap1
Tap2
Tapbp
Tapbpl
Psmb10
Psmb9
Psmb8
% Expressed
Average Expression

Figure 4

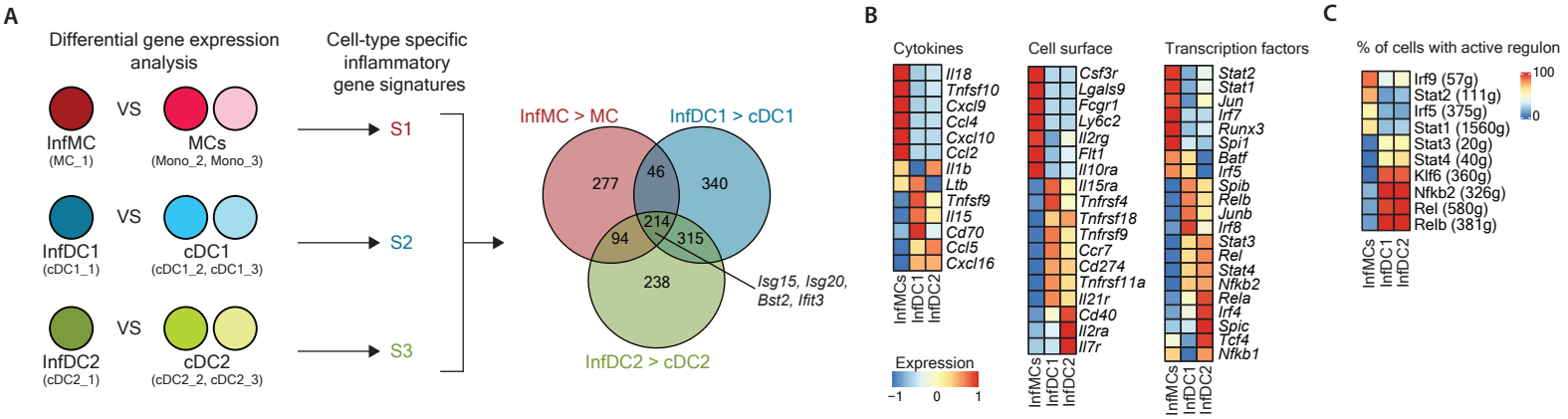
A
Differential gene expression analysis
Cell-type specific inflammatory gene signatures
InfMC
(MC_1)
VS
MCs
(Mono_2, Mono_3)
S1
InfDC1
(cDC1_1)
VS
cDC1
(cDC1_2, cDC1_3)
S2
InfDC2
(cDC2_1)
VS
cDC2
(cDC2_2, cDC2_3)
S3
InfMC > MC
InfDC1 > cDC1
InfDC2 > cDC2
277
46
340
214
94
315
238
Isg15, Isg20, Bst2, Ifit3
B
Cytokines
Il18
Tnfsf10
Cxcl9
Ccl4
Cxcl10
Ccl2
Il1b
Ltb
Tnfsf9
Il15
Cd70
Ccl5
Cxcl16
InfMCs
InfDC1
InfDC2
Expression
−1
0
1
Cell surface
Csf3r
Lgals9
Fcgr1
Ly6c2
Il2rg
Flt1
Il10ra
Il15ra
Tnfrsf4
Tnfrsf18
Tnfrsf9
Ccr7
Cd274
Tnfrsf11a
Il21r
Cd40
Il2ra
Il7r
InfMCs
InfDC1
InfDC2
Transcription factors
Stat2
Stat1
Jun
Irf7
Runx3
Spi1
Batf
Irf5
Spib
Relb
Junb
Irf8
Stat3
Rel
Stat4
Nfkb2
Rela
Irf4
Spic
Tcf4
Nfkb1
InfMCs
InfDC1
InfDC2
C
% of cells with active regulon
Irf9 (57g)
Stat2 (111g)
Irf5 (375g)
Stat1 (1560g)
Stat3 (20g)
Stat4 (40g)
Klf6 (360g)
Nfkb2 (326g)
Rel (580g)
Relb (381g)
100
0
InfMCs
InfDC1
InfDC2

Figure 5

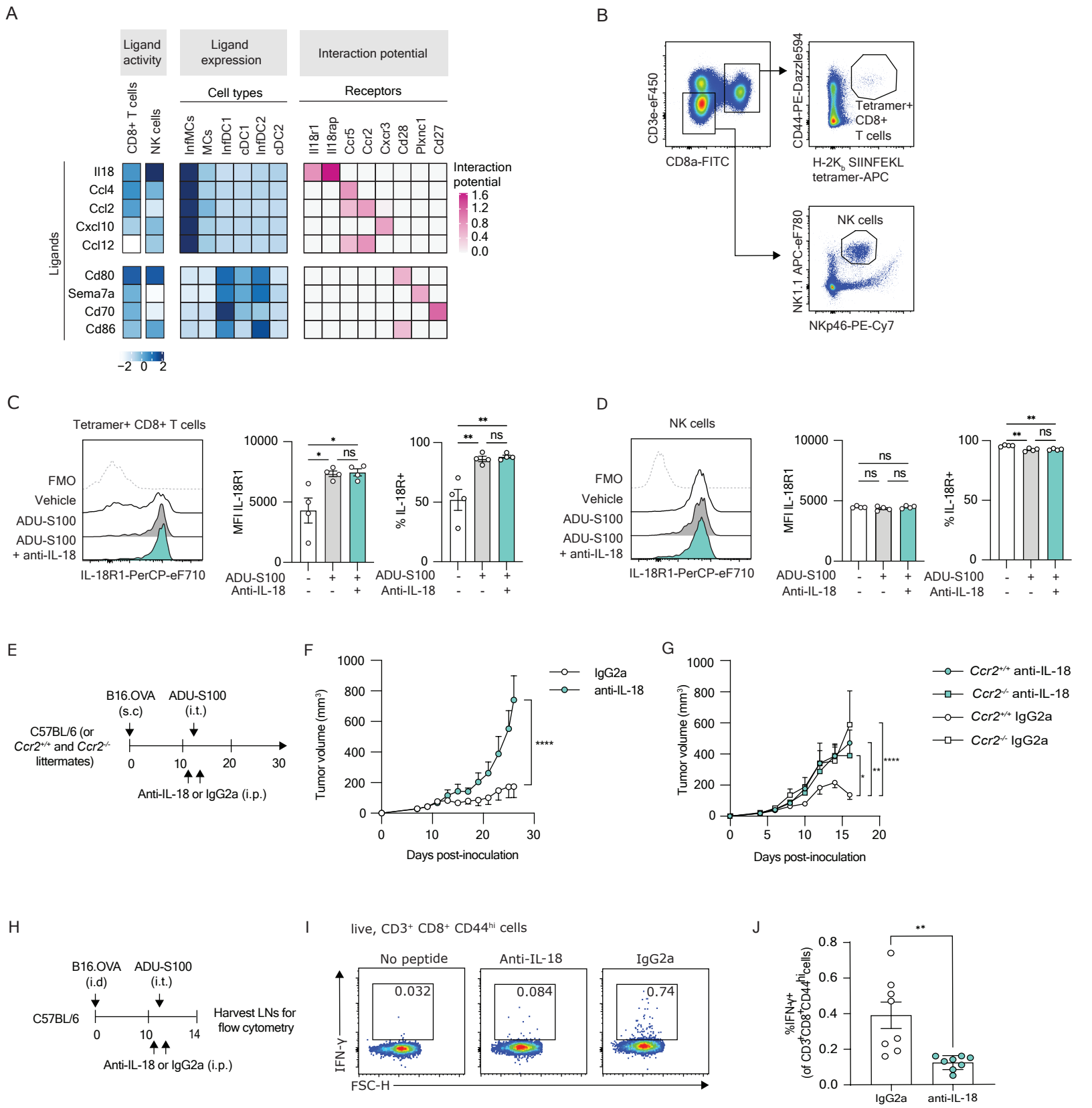
A
Ligand activity
Ligand expression
Interaction potential
CD8+ T cells
NK cells
Cell types
Receptors
InfMCs
MCs
InfDC1
cDC1
InfDC2
cDC2
Il18r1
Il18rap
Ccr5
Ccr2
Cxcr3
Cd28
Plxnc1
Cd27
Ligands
Il18
Ccl4
Ccl2
Cxcl10
Ccl12
Cd80
Sema7a
Cd70
Cd86
Interaction potential
1.6
1.2
0.8
0.4
0.0
−2 0 2
B
CD3e-eF450
CD8a-FITC
CD44-PE-Dazzle594
Tetramer+ CD8+ T cells
H-2Kb SIINFEKL tetramer-APC
NK cells
NK1.1 APC-eF780
NKp46-PE-Cy7
C
Tetramer+ CD8+ T cells
FMO
Vehicle
ADU-S100
ADU-S100 + anti-IL-18
IL-18R1-PerCP-eF710
MFI IL-18R1
% IL-18R+
ADU-S100
Anti-IL-18
ns
D
NK cells
E
B16.OVA (s.c)
ADU-S100 (i.t.)
C57BL/6 (or Ccr2+/+ and Ccr2-/- littermates)
Anti-IL-18 or IgG2a (i.p.)
F
Tumor volume (mm3)
Days post-inoculation
IgG2a
anti-IL-18
G
Ccr2+/+ anti-IL-18
Ccr2-/- anti-IL-18
Ccr2+/+ IgG2a
Ccr2-/- IgG2a
H
B16.OVA (i.d)
ADU-S100 (i.t.)
C57BL/6
Harvest LNs for flow cytometry
Anti-IL-18 or IgG2a (i.p.)
I
live, CD3+ CD8+ CD44hi cells
No peptide
Anti-IL-18
IgG2a
0.032
0.084
0.74
IFN-γ
FSC-H
J
%IFN-γ+ (of CD3+CD8+CD44hi cells)
IgG2a
anti-IL-18

Figure 6